JOURNAL OF PETROLOGY | VOLUME 37 | NUMBER 2 | PAGES 235–260 | 1996

ANTONIO CASTRO[1]*, CARLOS FERNANDEZ[1], JESUS D. DE LA ROSA[1], IÑAKI MORENO-VENTAS[1] AND GRAEME ROGERS[2]

[1]DEPARTAMENTO DE GEOLOGÍA, UNIVERSIDAD DE HUELVA, CAMPUS DE LA RÁBIDA, 21819 HUELVA, SPAIN

[2]SCOTTISH UNIVERSITIES RESEARCH AND REACTOR CENTRE, EAST KILBRIDE, GLASGOW G75 0QU, UK

Significance of MORB-derived Amphibolites from the Aracena Metamorphic Belt, Southwest Spain

The Aracena metamorphic belt, in the southwest Iberian Massif, is characterized by the presence of MORB-derived amphibolites and continental rocks deformed and metamorphosed during the Hercynian orogeny. Geochemical relationships of these amphibolites indicate the existence of a multiple fractionation process from a set of parental magmas, implying the existence of a multi-chamber system beneath the ridge where the basalt protolith was extruded. Neodymium isotopic ratios are typical of MORB, and oxygen isotopes indicate that these amphibolites have been derived from the uppermost part of the oceanic crust. Thermal evolution, revealed from the study of chemical variations in the amphibole chemistry, is interpreted as resulting from subduction in a low-pressure regime in which the thermal structure of the continental hanging-wall played an important role. This continental wall was previously heated by subduction of a slab window resulting from migration of a triple junction along the continental edge during plate convergence. Three petrologic arguments support this tectonic model. These are: (1) the low-pressure inverted metamorphic gradient of amphibolites of the oceanic domain; (2) the high-temperature–low-pressure metamorphism of the continental hanging wall; (3) the early intrusion of boninites into the continental domain.

KEY WORDS: *amphibolite; boninites; Hercynian belt; inverted metamorphic gradient; slab-window*

INTRODUCTION

Amphibolites are rocks of high petrologic interest as they are normally derived from igneous protoliths of tholeiite affinity that in many cases are recognized as fragments of old oceanic crust. Furthermore, amphibolitic complexes are of special relevance in the study of the thermal evolution of ancient orogenic belts, such as the Appalachian belt of North America, where the study of the metamorphism of amphibolitic rocks has resulted in several important reference works by Laird (1980), Laird & Albee (1981) and Spear (1982), among others, which have established thermal constraints on the conditions of metamorphism over a wide range of amphibole stability. In a similar way, the petrogenesis and thermal evolution of the amphibole-bearing units of the Aracena massif, Spain, have been investigated. The Aracena massif is a linear, high-temperature metamorphic belt (Bard, 1969) which marks an important suture zone in the Hercynian fold belt of Western Europe. The massif was extensively mapped by Bard (1969), but many questions related to the metamorphism and petrogenesis of the amphibolites have remained unsolved for more than 20 years. Bard reported the existence of an anomalously high-temperature metamorphic gradient. The Aracena area was mentioned by Miyashiro (1973, p. 176) as an example of a low-pressure metamorphic belt in which the transverse distance from the thermal axis, in granulite facies, to the biotite isograd is only 3–10 km. This is a ubiquitous feature of the Aracena massif, and the origin of this ultra-high-temperature gradient has important implications for the evolution of the southern sector of the Hercynian belt of Europe. However, the correct identification of this metamorphic gradient is difficult to determine because more than one episode of metamorphism and deformation has affected the Aracena massif; hence detailed studies are necessary to constrain the P–T conditions of the main metamorphic event. Detailed sampling and mapping has been carried out during

*Corresponding author.

the last few years, and the main results of this study are presented here. Two problems are addressed in this study: (1) the petrogenesis of the amphibolites; (2) the thermal evolution during the main stage of prograde metamorphism and deformation. On one hand, whole-rock geochemistry, including major and trace elements, and oxygen isotopes of the amphibolites are used to identify the nature of the igneous protolith. On the other hand, microprobe analyses, from plagioclases and ferromagnesian phases such as amphibole and pyroxene, are used to constrain P–T conditions. Furthermore, a detailed mapping and a structural study of a sector of the Aracena metamorphic belt has clarified the deformational history related to the thermal events that affected the area during the Hercynian orogeny. The results of this work provide important insights of crustal evolution and plate dynamics in the past.

REGIONAL SETTING OF THE ARACENA METAMORPHIC BELT

The Aracena metamorphic belt (AMB) constitutes the southernmost outcrop of high-grade rocks in the Ossa–Morena zone (OMZ), one of the main units forming the Iberian Massif, in the west of the European Hercynides (Fig. 1). This zone of the Iberian Massif is characterized by alternating linear metamorphic and plutonic belts (Bard, 1969) following the regional structural trend. The southern boundary of the OMZ is marked by an east–west-oriented shear zone [the South Iberian shear zone of Crespo-Blanc & Orozco (1988)] developed mainly within the southern part of an oceanic sheet (Acebuches amphibolites; Bard, 1969; Bard & Moine, 1979; Dupuy *et al.*, 1979) but also affecting an imbricate sequence of terrigenous sediments, serpentinites and metabasites (the Pulo do Lobo zone), interpreted as an accretionary prism (Eden, 1991). The Pulo do Lobo zone is located to the south of the amphibolite band and has been overthrust by them. These amphibolites are traditionally assigned to the OMZ, and constitute the southernmost limit of the Aracena metamorphic belt. Although their metamorphic and structural characteristics are in agreement with this somewhat rigid division, clearly the complex tectono-thermal evolution of this unit must be deciphered before a complete, more dynamic picture can emerge. Following the seminal work by Bard (1969), the geological exploration of the AMB remained neglected for many years, until more recent studies recognized the exceptional geotectonic significance of this sector of the European Hercynides (e.g. Crespo-Blanc & Orozco, 1988; Eden, 1991; Quesada *et al.*, 1994).

METAMORPHIC DOMAINS AND STRUCTURE OF THE ARACENA METAMORPHIC BELT

The main feature of the Aracena metamorphic belt (AMB) is the linear disposition of metamorphic zones, which in some cases are bounded by ductile faults which post-date the main episode of deformation and metamorphism. These zones have distinctive lithological, structural and metamorphic characteristics and, though they can be integrated within a unique process of crustal reactivation during the Hercynian event, they can be considered separately so as to simplify the descriptions. We prefer to refer to these zones as domains, as they show considerable internal coherence as a result of a common process of deformation and metamorphism. Two main domains can be distinguished in the AMB (Fig. 2): (1) the southern (oceanic) domain, composed of amphibolites and mafic schists interpreted as derived from metamorphism of an oceanic crust (Dupuy *et al.*, 1979); (2) the northern (continental) domain, composed of continental pelitic and calc-silicate gneisses with intercalated marbles, amphibolites (the Rellano amphibolites) and mafic granulites.

The oceanic domain (OD) is composed primarily of amphibolites with subordinate metadolerites and mafic schists. These amphibolites outcrop as a long (>100 km), narrow (~ 1 km) band with a rough east–west azimuth and dipping $>50°$ to the north. This band is disrupted by late, brittle strike-slip faults (Fig. 1b). To the north, the amphibolitic band is in contact with the continental domain of the AMB. To the south, it overlies the Pulo do Lobo zone, recently interpreted as an accretionary prism as mentioned above. The present thickness of the amphibolitic pile is ~ 600 m in the studied area.

Three main deformational phases can be identified in this domain. The first phase (OD-D_1), coincident with the main metamorphic stage, is very penetrative and is responsible for the development of a metamorphic banding and foliation. The intensity of this fabric and the grain size increase towards the top. Structural analysis points to a non-coaxial deformation regime for OD-D_1, and reveals a complex kinematic frame, with a top-to-the-south thrust component, and a sinistral strike-slip component (Fig. 3). During the second phase (OD-D_2) ductile shear-zones are developed which have par-

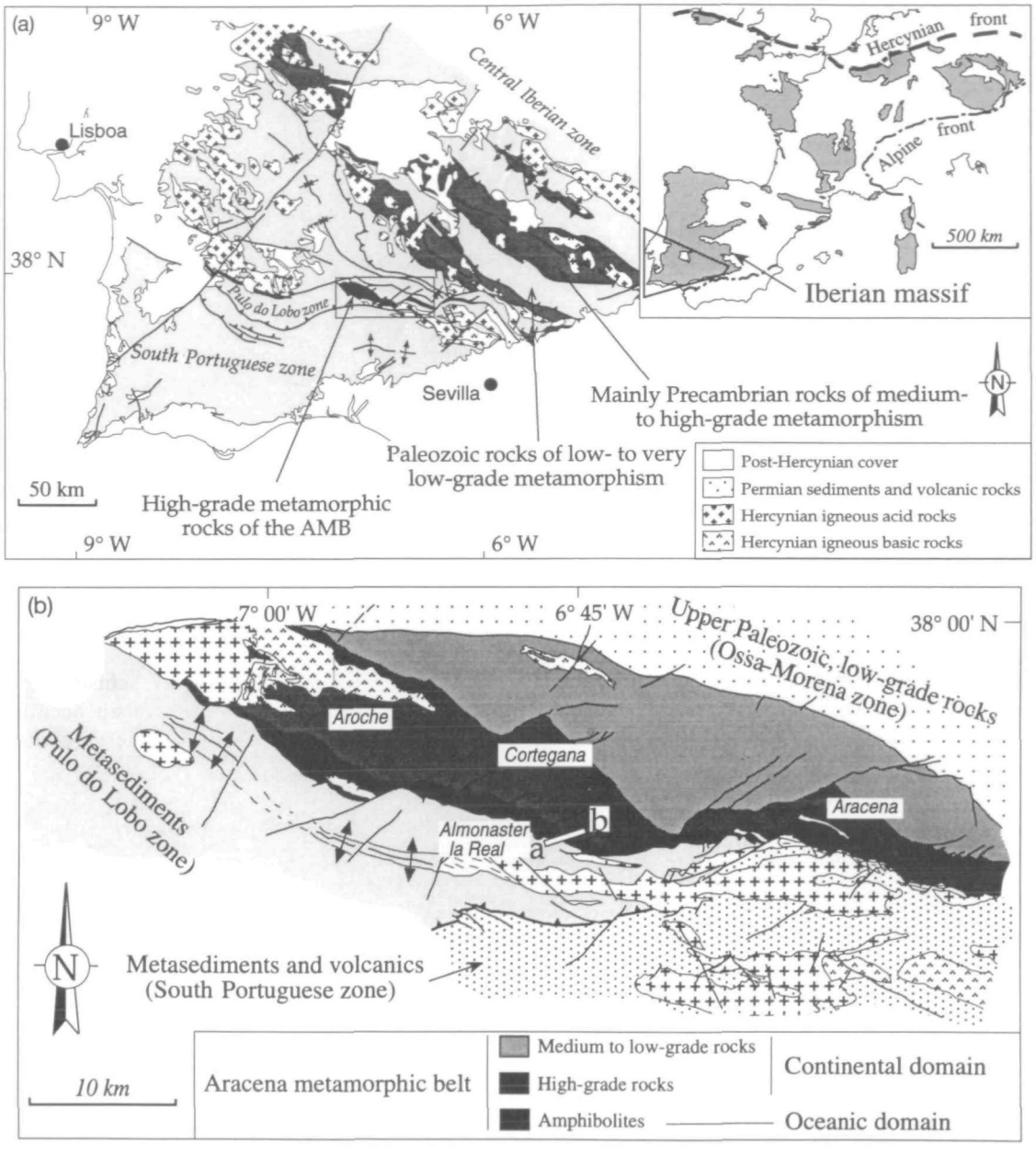

Fig. 1. (a) Sketch of the southernmost part of the Iberian Massif, showing the distribution of metamorphic belts in the Ossa–Morena zone [division by Julivert *et al.* (1974) and Quesada (1991)]. The inset depicts the location of this area in the context of the western European Hercynides. (b) Simplified geological map of the Aracena metamorphic belt and adjacent areas [division after Crespo-Blanc (1987)].

ticularly affected the bottom of the amphibolite pile, where >150 m of mylonites can be recognized (Crespo-Blanc & Orozco, 1988). However, an anastomosing network of thinner shear bands traverses the entire amphibolite pile, isolating fish-shaped portions of less deformed rock. The OD-D_2 develops a retromorphism over the amphibolites to greenschist facies (mafic schists with actinolite–chlorite), which overprints several facies of the previous metamorphism. The kinematics of the second deformational phase is similar to that of the first one, but with a stronger strike-slip component (Fig. 3). A third, ductile phase of deformation (OD-D_3) produced the shear zones which locally appear at the boundary between the oceanic and continental domains. These are centimetre- to metre-scale shear bands, producing a strong mylonitization and retromorphism of high-grade amphibolites. Locally, they

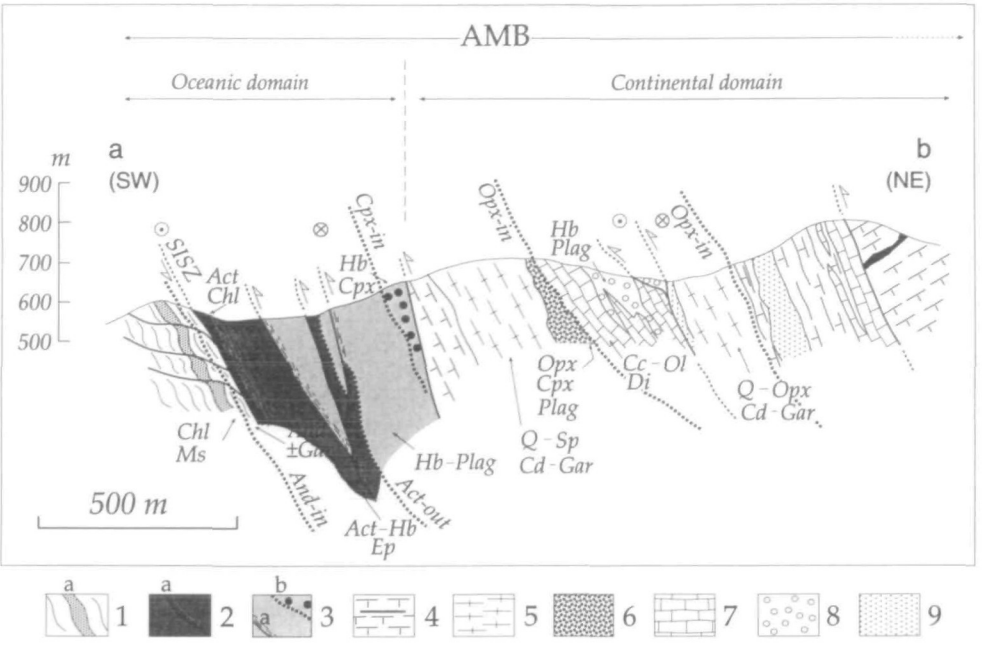

Fig. 2. Cross-section of the southern part of the Aracena metamorphic belt. Metamorphic isograds are represented as thick discontinuous lines. 1, Pulo do Lobo metasediments; a, massive quartzites. 2, Act–Hb–Ep amphibolites; a, Act–Chl schists related to the second phase of deformation and metamorphism. 3, Hb amphibolites; a, Act–Chl schist (same meaning as in 2); b, Hb–Cpx amphibolites. 4, Calc-silicates with occasional metabasites. 5, Pelitic granulites and gneisses. 6, Mafic granulites. 7, Marbles. 8, Rellano amphibolites. 9, Leucocratic gneisses.

penetrate the continental domain, leaving intact the original, pre-shearing contact between the amphibolites and continental rocks. The kinematic indicators in the shear zone (Fig. 3) suggest a top-to-the-south thrust motion.

The complex succession that characterizes the continental domain was folded and metamorphosed during the main phases of the Hercynian orogeny. In the southern part of the CD metamorphism reached granulite facies at low pressure (Bard, 1969). In contrast, towards the north, the CD is characterized by the presence of a medium- to low-grade metamorphism affecting a terrigenous series with abundant acidic and basic metavolcanics. This terrigenous–volcanic composite series overlies Cambrian carbonates (Aracena dolomites) and these in turn are situated over Precambrian terrigenous series (La Umbría series).

The first deformational phase in the continental domain (CD-D_1) generated a regional, penetrative, axial plane foliation associated with large, southwards vergent folds. The original attitude of both foliation and folds is difficult to ascertain as the later deformations produced complex interference patterns, with local reorientation of the previous structures. Nevertheless, a subhorizontal or gently north-dipping position can be deduced from cartographic arguments. Coeval with the first deformational phase is a low-P metamorphism whose thermal peak, represented by low-pressure–ultra-high temperature (~900°C and 3 kbar) gneisses, is late with respect to the main phase of folding. It is important to note that the metamorphic zonation within the CD is asymmetrical. The highest temperature zone occurs in the south, in contact with the amphibolites of the oceanic domain. This high-T zone, with pelitic and mafic granulites and high-temperature amphibolites (Rellano amphibolites), defines a band parallel to the oceanic domain but oblique to the structural trend of the CD, in such a way that the main lithologies appear metamorphosed at different degrees from east to west. Towards the north, the low-P metamorphism evolves from granulite to amphibolite and finally to greenschist facies. Several ductile shear zones indicating either strike-slip or normal senses of motion appear across the CD.

ROCK TYPES AND FIELD RELATIONSHIPS

Metabasites of the oceanic domain

The oceanic domain of the AMB is composed of a thick pile of amphibolites, which have very few exotic components such as metasomatic nodules and some pelitic layers associated with a late episode of

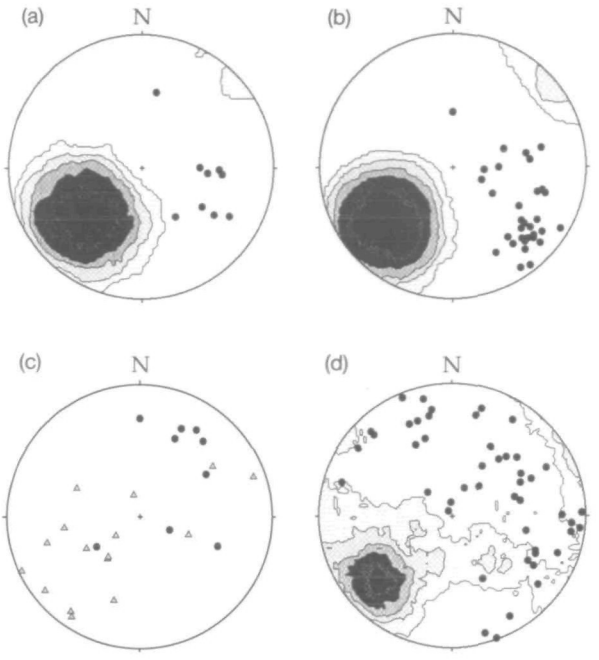

Fig. 3. Structural diagrams of the AMB. Equal-area, lower-hemisphere projections. Contour densities of poles to foliation. Uniform distribution: 3σ. Dots: mineral or mylonitic lineation. (a) First phase, oceanic domain. Contour interval: $1{\cdot}4\sigma$. Number of foliation poles: $n=49$. Mineral lineation: $n=9$. (b) Second phase, oceanic domain. Contour interval: $1{\cdot}65\sigma$. Mylonitic foliation: $n=47$. Stretching lineations: $n=32$. (c) Third phase, oceanic domain and second phase, continental domain. Triangles: mylonitic foliation, $n=16$. Dots: mineral and stretching lineations, $n=10$. (d) First phase, continental domain. Contour interval: $1{\cdot}28\sigma$. Foliation: $n=285$. Mineral lineation: $n=47$.

deformation and retrogression. Previous work by Bard & Moine (1979), as well as the data included in this paper on the geochemistry of these amphibolites, clearly supports the idea that they represent metamorphosed tholeiitic basalts of MORB affinity. This feature gives the AMB a special significance in the geotectonic interpretation of the Hercynian chain of Iberia. Several geotectonic models have been proposed (e.g. Abalos *et al.*, 1991; Bard, 1992; Quesada *et al.*, 1994) in recent years, but none accounts for the complex metamorphic evolution of the amphibolite pile.

The following rock units can be distinguished according to textural and mineralogical criteria: (1) amphibolites; (2) mafic schists; (3) metadolerites. These rock units are disposed in parallel bands, elongated following the regional trend of structures (east–west to NW–SE). Within the group of amphibolites, two main types may be distinguished according to common assemblages: (1) normal amphibolites, composed of amphibole–plagioclase, which dominate the oceanic domain of the AMB; (2) quartz-rich amphibolites, which are interlayered with the former and are composed of quartz–diopside–plagioclase–amphibole. Figure 4 shows the typical aspect of layered amphibolites with quartz-rich facies intercalated with normal amphibolites.

In zones with low-grade metamorphism and low deformation there are bands in which a relict magmatic texture may be recognized. These are metadolerites that may contain relict phenocrysts of augite and plagioclase. These metadolerites appear as lens-shaped bodies (10–30 cm in size) bounded by anastomosing shear bands. They are mainly located towards the south of the pile. The foliation of the OD-D_1 is parallel to a characteristic layering in which fine-grained amphibolites alternate with medium- to coarse-grained amphibolites. The only difference between the two types is the grain size and not the composition as in the case of the layering shown in Fig. 4, and referred to above.

Figure 5 shows the distribution of facies and structures in a typical section across the amphibolite pile near the locality of Almonaster. The main episode of metamorphism is associated with OD-D_1, indicating a top-to-the-south directed thrusting, and a sinistral strike-slip component, as based on meso- and microstructures observed in the rocks. This grade of metamorphism increases towards the north, reaching the transition to the granulite facies near the contact with the continental domain. As the main foliation dips towards the north, the metamorphism appears inverted, with the amphibolite–granulite facies transition at the top of the metamorphic pile. This is a peculiar feature of the AMB and will be discussed below.

The mafic schists are chlorite–actinolite–albite schists developed in discrete shear bands affecting the pre-existing amphibolites. They represent the second episode of metamorphism and deformation (OD-D_2). The most important feature of this shearing phase is that it occurred under low-grade conditions producing a local retrogression in the amphibolites. In places, hornblende amphibolite bands are preserved. As the main objective of this study is to analyse the first episode of metamorphism, these mafic schists are not discussed.

Metabasites of the continental domain

Intercalated within the marbles and calc-silicates of the continental domain there are tabular bodies (10–200 m thick) of very coarse-grained amphibolites, called the Rellano amphibolites. Hornblende crystals are normally >2 cm in length. Occasionally, in irregular pockets, the major length may reach >10 cm. These coarse-grained amphibolites are isotropic

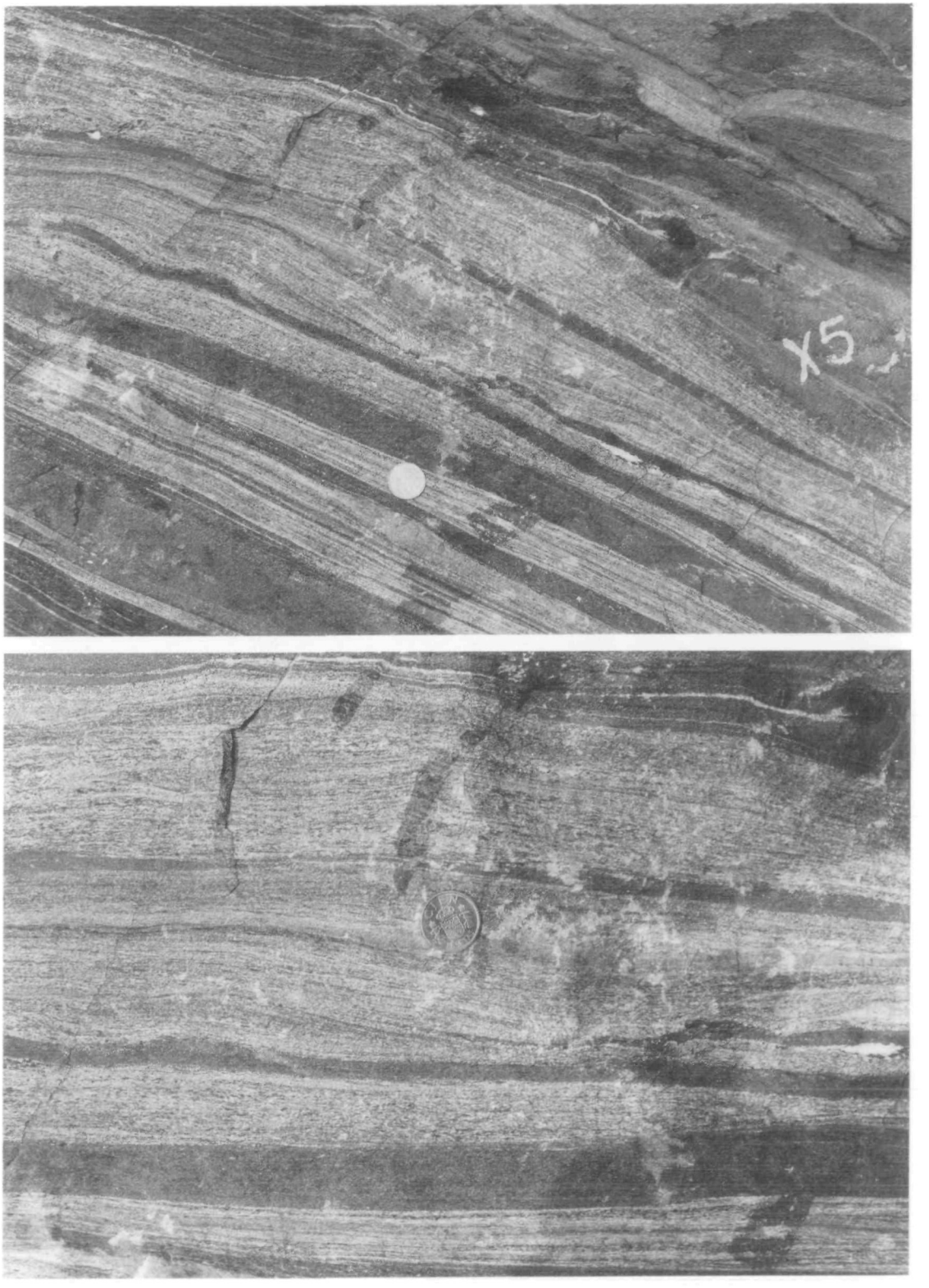

Fig. 4. Mesoscopic aspect of layered amphibolites from the Hb zone.

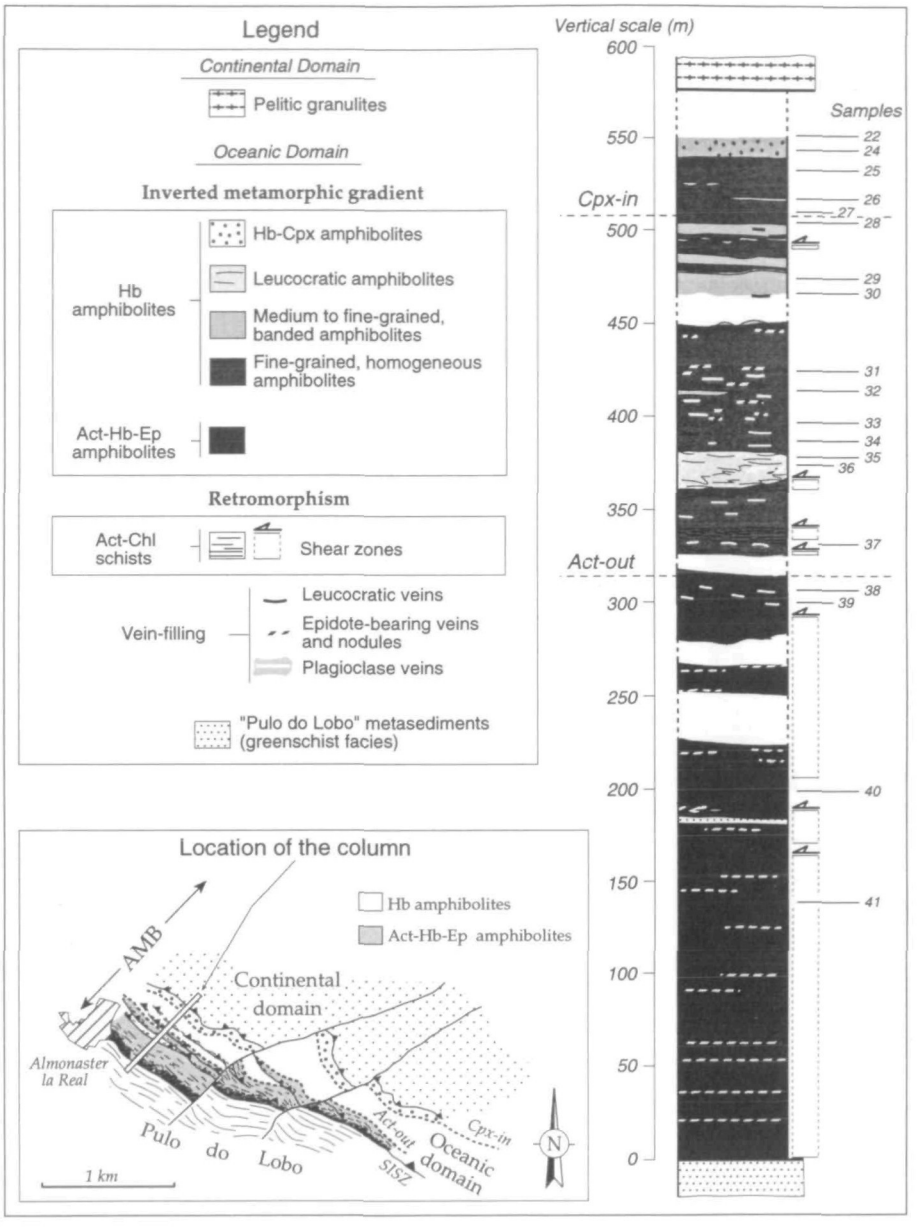

Fig. 5. Schematic profile of amphibolites from the oceanic domain near the village of Almonaster la Real (see inset for location).

rocks, not affected by the main episode of regional deformation of the continental domain.

Other metabasites outcropping in the continental domain are mafic granulites which appear as kilometre-sized, irregular bodies crosscutting the main foliation of the leucocratic and pelitic gneisses within which they are enclosed. These rocks are always isotropic, with no apparent foliation. They constitute premetamorphic intrusions of mafic magmas that are late with respect to the main episode of regional deformation of the continental domain, but earlier than the metamorphic peak. These relationships are important in interpreting the tectonothermal evolution of the AMB.

PETROGRAPHY

The normal amphibolites of the oceanic domain are generally composed of plagioclase–amphibole ± clinopyroxene ± sphene ± epidote ± ilmenite ± magnetite ± quartz ± apatite, with amphibole and plagioclase constituting >90 vol. % of the rock. Despite such compositional homogeneity there are important variations in grain size. In general,

coarse-grained amphibolites (>4 mm) are mo abundant near the top of the pile in the Hb–C zone, where they appear as narrow bands (5–50 cr intercalated with medium-grained (1–4 mr amphibolites. The contacts are sharp and there a no compositional differences between these alte nating bands. Medium-grained (1–4 mm) amphib lites dominate the metamorphic pile in the Hb zo and evolve towards the south, in the Act–Hb zon to fine-grained (<1 mm) amphibolites alternating narrow bands (2–20 cm) with zones of retrogressi where the amphibolites have been transformed in chlorite–actinolite schists. Independent of the gra size, the amphibolites have a well-developed met morphic foliation parallel to the granulometric layering. This feature, together with the lack of compositional differences between layers, suggests that the foliation and layering developed at the same time during the main episode of metamorphism and deformation (OD-D_1), the coarse-grained bands perhaps representing zones richer in fluids compared with adjacent zones poorer in fluids that developed high-nucleation density textures.

Table 1 summarizes the main petrographic variations with distance in the normal amphibolites from the oceanic domain. In the Hb–Cpx zone, at the top of the amphibolite pile (Figs 2 and 5), the common assemblage is plagioclase–hornblende–clinopyroxene with subordinate sphene, ilmenite and magnetite. Plagioclase shows a continuous zoning ranging from An_{50} at the rim to An_{65} at the core. The amphibole is brown to green hornblende occasionally zoned with a brown core and a dark green rim. The grain boundaries between this amphibole and the clinopyroxene (diopside) are sharp with no signs of reaction between the phases. Locally, diopside may show reaction textures to an actinolitic amphibole, probably related to the retrogression that affected the amphibolite pile.

The change in the colour of the amphiboles which define the main foliation is related to the amphibole composition, which, in turn, reflects temperature. This feature was first recognized by Bard (1969). Amphiboles evolve from a yellowish green colour at the bottom through dark green to brown at the top of the pile. The change from green to brown is roughly coincident with the appearance of diopside. This change is mainly related to the titanium content of the amphibole, but other compositional variations are also involved, as revealed by microprobe analyses. These changes clearly indicate an increase of metamorphic temperature from the bottom to the top of the amphibolite pile.

Another petrographic feature of the amphibolites in the Act–Hb and Hb zones of the OD is the presence of relict igneous phases such as plagioclase and augite, supporting the igneous nature of the amphibolite protolith. Relict plagioclases are characterized by the presence of oscillatory zoning in the cores of porphyroblasts. These normally appear fragmented and contoured by the main foliation defined by amphibole and new plagioclase. Figure 6 shows the typical aspect of one of these relict plagioclases.

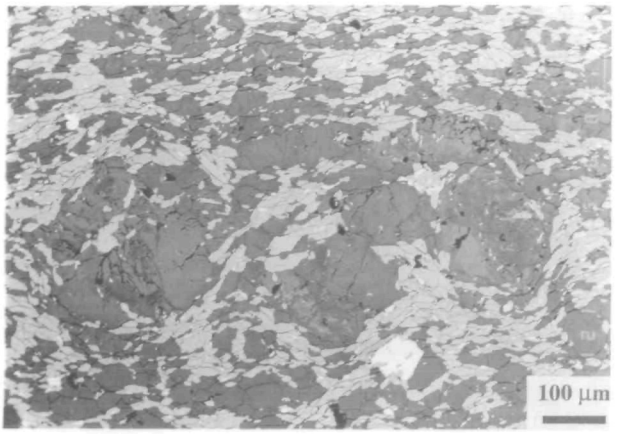

Fig. 6. Back-scattered electron images (Z-contrast) showing the zoning in plagioclase with relict cores. The brighter zones are remnants of calcic cores as revealed by the BSE (Z-contrast) image. Such zones are free of amphibole inclusions, these being abundant in the darker zones, which represent the new plagioclase formed in the course of metamorphism.

The Rellano amphibolites appearing in the continental domain are characterized by the very coarse grain size and the dark brown colour of the amphiboles. The texture is typically granoblastic with abundant polygonal junctions between plagioclases and between plagioclase and amphibole. They are composed of brown hornblende–plagioclase ± sphene ± clinopyroxene ± ilmenite.

Finally, the mafic granulites of the CD are characterized by the assemblage clinopyroxene–orthopyroxene–plagioclase–quartz ± ilmenite ± magnetite and the retrograde phases biotite and amphibole developed as a corona reaction after orthopyroxene. These granulites are not deformed and show a typical granoblastic texture between ortho- and clinopyroxene. Plagioclase normally appears as centimetre-sized, poikiloblastic crystals enclosing the pyroxenes. Though these rocks normally have metamorphic textures, many facies retain their original igneous textures, the mineral assemblage being essentially the same. These igneous facies are important, as they indicate the igneous provenance of these mafic bodies.

MINERAL CHEMISTRY

Plagioclase, amphibole and pyroxene have been

Table 1: Summarized petrography of normal amphibolites from the oceanic domain, showing the main variations across a complete section of the amphibolite pile

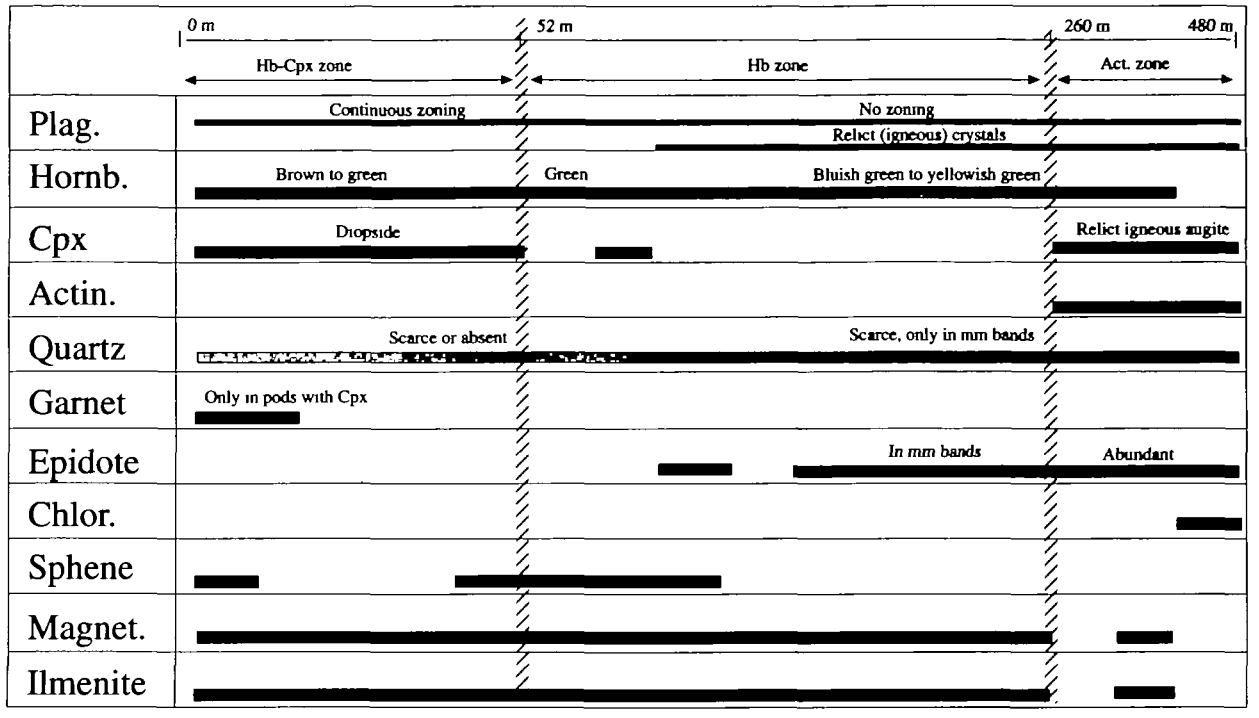

analysed by electron probe microanalysis (EPMA) to constrain P–T conditions during metamorphism. Pressure may be estimated from the composition of pyroxene in equilibrium with quartz in the quartz-bearing amphibolites. Plagioclase–amphibole pairs are used to identify equilibrium conditions, and finally the chemistry of amphibole may be useful to obtain some information on the P–T trajectories. Zoned amphiboles have been analysed to constrain P–T variations during metamorphism in the continental domain and to compare these variations with the results obtained from similar zoning patterns in amphiboles of the oceanic domain.

Representative samples of amphibolites from the oceanic and continental domains have been analysed by EPMA, mainly for amphibole, plagioclase and clinopyroxene. Several samples of the Rellano amphibolites from two distinct localities of the continental domain have been collected. A set of 24 samples has been collected from amphibolites of the oceanic domain in a 550 m traverse perpendicular to the foliation, from the Act–Hb zone to the Cpx–Hb zone (Fig. 5, Table 1). Quartz amphibolites have been excluded from this study to keep the compositional variable constant. These have a very homogeneous whole-rock composition (Table 2), and variations in the amphibole compositions may be related to changes in the P–T conditions.

Bard (1969) divided the Aracena metamorphic belt into three main domains based on the colour of amphiboles in metabasites, including amphibolites appearing in the continental domain. Variations from green–blue through green to brown occur in the oceanic domain in a section of ~500 m, denoting a very high thermal gradient. The study of these variations is critical in understanding the metamorphic evolution of the AMB.

Selected samples were analysed by EPMA (Cameca Camebax) at the University of Oviedo (Spain) and by EPMA (JEOL Superprobe 733) at the University of St Andrews (Scotland). Operating conditions were similar in both laboratories, with a probe current of 20 nA and an accelerating voltage of 15 kV. Standards were in both cases a combination of pure metals, oxides and minerals, with the application of ZAF correction procedures. The results were checked, giving a high degree of reproductivity between the two laboratories. Special emphasis was placed on amphiboles but other coexisting phases such as plagioclases and pyroxenes have been also analysed to determine the pressure and temperature conditions during metamorphism.

Table 2: Average chemical composition of normal amphibolites and typical MORB

Rock type:	Normal amphibolite			1	2
	Av.	Max.	Min.		
SiO_2	49·28	51·50	47·80	49·30	49·43
TiO_2	1·17	1·58	0·53	1·80	1·62
Al_2O_3	16·43	20·60	14·50	15·20	15·97
Fe_2O_3	—	—	—	2·40	2·09
FeO	—	—	—	8·00	7·55
Fe_2O_{3T}	9·07	11·30	5·60	—	—
MgO	7·22	8·38	5·19	8·30	8·50
MnO	0·17	0·23	0·11	0·17	0·18
CaO	11·56	12·70	5·23	10·80	10·73
Na_2O	2·83	3·66	2·34	2·60	2 87
K_2O	0·18	0·54	0·01	0·24	0·18
P_2O	0·14	0·21	0·05	0·21	0·15
LOI	1·01	3·10	0·46	—	—
Total	99·04			99·02	99·27

1, Oceanic tholeiite (Hyndman, 1972); 2, amphibolite (Spear, 1981).

Amphibole

Representative amphibole analyses are listed in Table 3. The schemes of Robinson *et al.* (1982) were used for formula normalization. The calculation of the oxidation state in amphiboles is crucial for a complete estimation of site occupancy, especially the Na occupancy in the M4 site. Any procedure based on stoichiometric constraints is inaccurate, as the amphibole formula may have vacancies in the A site and in the eight-fold coordinated M4 site, making the stoichiometric recalculation dependent on assumptions on site occupancy. It is apparent that the ferric:ferrous iron ratio is strongly dependent on the f_{O_2} of the system and it may be evaluated if the oxygen fugacity is determined in other complementary ways.

The experimental work of Spear (1981) established a correlation between the oxygen fugacity and the composition of amphiboles by running several experiments on MORB-derived amphibolites at different oxygen fugacities fixed by the three buffers wüstite–magnetite (WM), quartz–fayalite–magnetite (QFM) and haematite–magnetite (HM). The results are not of general applicability, as bulk composition and temperature condition the f_{O_2} in the system. However, in our case these experimental data can be used as a good guide for ferric iron estimations in the amphibole molecule for the following reasons: (1) the rock used by Spear (1981) in the experiments is very close in composition to the amphibolites of this study (Table 2); (2) the P–T conditions of the experimental work by Spear (1981) are comparable with the P–T range of the studied amphibolites. Cation proportions in the structural formulae, independent of the ferric iron recalculation, compared with the amphibole compositions obtained on three different buffers in Spear's (1981) experiments, indicate that the Aracena amphiboles crystallized under conditions of f_{O_2} around the QFM buffer. Furthermore, these amphibolites are derived from a MORB protolith and most terrestrial basalts have oxygen fugacity fixed around the QFM buffer (Carmichael & Nicholls, 1967; Blundy *et al.*, 1991), conditions that possibly were maintained during the metamorphic process.

Moreover, as reported experimentally by Moody & Jenkins (1983), oxygen fugacity determines the stability of some minor minerals such as sphene, epidote, ilmenite, magnetite, rutile and haematite in mafic systems, epidote and haematite being characteristic of the most oxidizing regimes. In these experimental runs (Moody & Jenkins, 1983), the assemblage sphene–ilmenite–magnetite was found when oxygen fugacities were around the QFM and nickel–nickel oxide (NNO) buffers. At the QFM

Table 3: Representative microprobe analyses of amphiboles

Rock type:	Cpx–Hb amphibolites			Hb amphibolites			Act–Hb amphibolites			Rellano		
Sample:	893-22-9	893-24-12	893-25-3	893-28-4	893-30-9	893-31-5	893-39-8	893-40-2	893-41-1	89227-4	89227-7	89227-10
SiO_2	47·39	45·89	44·64	46·05	45·58	47·25	47·28	48·14	52·56	47·63	46·71	44·15
TiO_2	1·00	1·16	1·68	1·55	1·19	1·16	0·73	1·44	0·16	0·87	1·27	1·56
Al_2O_3	7·07	8·37	8·94	8·69	8·48	7·24	7·02	7·79	3·37	8·20	8·06	9·63
Fe_2O_3*	2·02	2·19	2·24	1·98	2·33	2·28	2·14	2·06	1·45	1·98	1·96	2·13
FeO	12·75	13·84	14·14	12·51	14·72	14·41	13·48	12·98	9·17	12·46	12·39	13·45
MnO	0·33	0·26	0·21	0·33	0·44	0·30	0·31	0·26	0·29	0·28	0·20	0·35
MgO	12·18	11·88	11·50	12·30	11·13	11·97	12·02	12·91	15·54	13·82	13·55	11·95
CaO	11·92	12·11	11·98	11·88	11·80	11·79	12·33	10·66	12·56	11·77	11·45	11·81
Na_2O	0·88	0·72	1·74	1·04	1·18	1·04	0·62	1·11	0·16	1·61	1·58	2·10
K_2O	0·33	0·08	0·11	0·12	0·09	0·06	0·66	0·09	0·10	0·07	0·08	0·17
Total	95·89	96·49	97·18	96·46	96·94	97·50	96·60	97·45	95·37	98·69	97·24	97·31

*Fe_2O_3 = 12·5% FeO_t.

buffer, sphene occurs as a low-temperature product whereas ilmenite–magnetite are high-temperature products. The common oxide assemblage of the AMB amphibolites is ilmenite–magnetite, ilmenite being very poor in titano-haematite (<5% mol). Sphene is present in all the amphibolites from the oceanic domain. According to these constraints, we have adopted a recalculation procedure based on a fixed proportion of ferric iron of 12·5% of the total iron, the composition of the amphiboles buffered around the QFM buffer, measured with the probe, for all the amphiboles studied in this paper, according to the experimental data of Spear (1981). The quartz-rich amphibolites and other metabasites of the AMB probably do not fit this constraint, as they have compositions that are different from that of the experimental runs of Spear (1981). Using these constraints for the ferric iron recalculation, an approach can be made to the cation allocations in the structural sites of the amphibole molecule following the scheme of Robinson *et al.* (1982). This procedure allows one to determine the occupancy in the A site and the application of the classification scheme of Leake (1978) modified by Pe-Piper (1988) presented in Fig. 7.

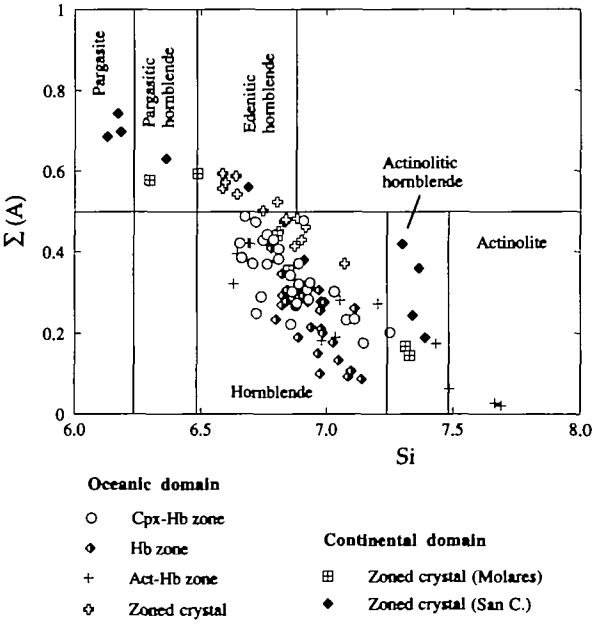

Fig. 7. Leake's (1978) classification diagram for amphiboles [modified by Pe-Piper (1988)] plotting amphiboles from the oceanic and continental domains of the Aracena metamorphic belt. (Note that pargasite and edenite dominate the composition of the cores of zoned amphiboles from the Rellano amphibolites.)

The best correlation is between Ti and tetrahedral Al, denoting the relative importance of the Ti-Tschermak (Ti-Ts) exchange $Al_2^{IV}TiMg_{-1}Si_{-2}$. Also, there is a good correlation between Al^{IV} and A-site occupancy, denoting the edenite-type (Ed) exchange $Al^{IV}Na(A)Si_{-1}\square_{-1}$. These two exchanges account for most of the four-fold co-ordinated Al. An assessment of the relative importance of the glaucophane exchange (Gl) is difficult as Na(M4) is dependent on the ferric-iron recalculation. Consequently, its relative importance is poorly constrained by this method of cation correlation. It can, however, be estimated by calculation of the glaucophane and other molecules in the amphibole space composition (see the Appendix).

Figure 8a shows a molecular plot relating the

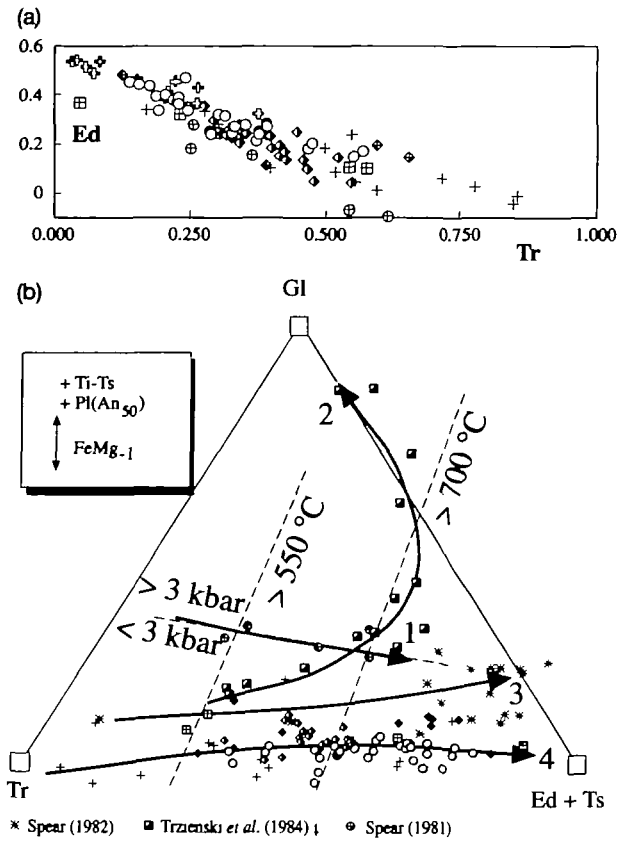

Fig. 8. (a) Molecular plots relating the additive component tremolite (Tr) to the end-member edenite (Ed). These molecules are calculated from algebraic transformation of the amphibole space composition (see Appendix). For comparative purposes, the amphiboles from the experimental runs at 3 kbar by Spear (1981) have been included in the plots (encircled crosses). Other symbols as in Fig. 7. (b) Baricentric projection of the analysed amphiboles in the space Tr–Gl–Pg (Ed + Ts) through the $FeMg_{-1}$ interchange and from Pl (An_{50}). Curve 4 marks the compositional evolution of the Aracena amphiboles (symbols as in Fig. 7). Other amphiboles are plotted for comparative purposes; these are: 1, experimental data at 3 kbar of Spear (1981); 2, zoned amphiboles of Trzienski *et al.* (1984); 3, zoned amphiboles of Spear (1982). Isotherms and isobars are tentatively traced following the experimental data of Spear (1981) as a guide. The model reproduces the anomalous cooling with increasing pressure referred to by Trzienski *et al.* (1984).

molecules of Ed calculated for the Aracena amphiboles to the additive component tremolite (Tr). This figure confirms the importance of the Ed-type substitution in our amphiboles, implying that the main compositional variation is related to temperature (Blundy & Holland, 1990). The Gl content is nearly constant for amphiboles which equilibrated at different temperatures. Also included in this plot are the experimental data of Spear (1981) for amphiboles synthesized at temperatures from 551 to 763°C at 3 kbar constant pressure. The Gl contents of these experimental amphiboles are higher than those of the AMB amphiboles, indicating that the confining pressure was <3 kbar in both the oceanic and continental domains of the AMB. Furthermore, the compositional variation displayed by a single zoned crystal is coincident with the variation displayed by amphiboles from different samples collected across the amphibolite pile (Fig. 8a).

Figure 8b is a baricentric projection of the amphibole–plagioclase space composition, projected from Pl (An_{50}), Ti-Ts and through the $FeMg_{-1}$ interchange. As Ed and Ts are strongly dependent on temperature (e.g. Spear, 1980, 1981; Blundy & Holland, 1990) they are plotted together as a pargasite molecule in the right-hand corner. Gl is plotted in the upper corner; as this molecule is strongly dependent on pressure, the figure may be taken as a distorted P–T diagram in which it is possible to identify the shape of any P–T path linking data points from a zoned amphibole or from a set of samples from a graded massif. Isotherms and isobars are tentatively traced taking as a reference the constant-pressure experimental data at 3 kbar of Spear (1981). The path depicted by the Aracena amphibolites is nearly horizontal and within the low-pressure region of the diagram. For comparative purposes, other paths obtained from zoned amphiboles from other metamorphic belts are also shown. This diagram reproduces the effect of increasing pressure during cooling reported by Trzienski *et al.* (1984) and deduced from a zoned crystal.

Zoned amphibole crystals from the oceanic and continental (Rellano amphibolites) domains display a characteristic P–T pattern on the baricentric projection Tr–Gl–(Ed + Ts). According to this pattern, zoned amphiboles record a first episode of increasing temperature marked by an appreciable increment in the Ed + Ts content, and a second episode of cooling denoted by an increase in the Tr content. Both episodes occurred at low pressure, this being the more salient feature of the thermal evolution of the Aracena metamorphic belt.

Amphibole–plagioclase relationships

Plagioclase is, together with amphibole, the dominant phase in the amphibolites of the oceanic domain. As indicated in Table 1, two distinct types of plagioclase may be distinguished according to the grain size and composition. Type I plagioclase has the same grain size (1–4 mm) as coexisting amphibole, with which it shows polygonal contacts. This indicates the existence of textural, and probably chemical, equilibrium between the two phases, as they grew at the same time under the same P–T conditions. This type shows slight changes in com-

position (An_{42}–An_{60}) from the Hb–Act zone to the Cpx–Hb zone. Type II are large crystals (1–4 mm) characterized by the presence of an anorthite-rich (An_{60-70}), igneous core with oscillatory zoning. This core is free of amphibole inclusions. The rim has a composition identical to that of the matrix plagioclase at around An_{40-50}. Figure 6 shows a back-scattered electron (BSE) scanning electron microscope image illustrating these relationships between plagioclase and amphibole. It can be appreciated that the amphiboles defining the foliation are intergrown with plagioclase of the matrix as well as with the outer rim of the type II plagioclases. This implies that these outer rims re-equilibrated during the course of metamorphism as part of the plagioclase is derived by 'retrogression' of an igneous, anorthite-rich plagioclase. The matrix plagioclases have been analysed with the probe near the contacts with adjacent amphibole crystals. Representative analyses are listed in Table 4. The relationships between coexisting amphibole and plagioclase indicate that equilibrium only existed at the local scale, as pairs from the same sample have distinct slopes. This observed local equilibrium is probably related to the compositional variability of relict plagioclases. Amphibole may grow in two different local situations in a reduced rock volume: (1) amphibole grown together with plagioclase during a prograde reaction after a lower-grade assemblage (e.g. Act–Ab–Ep); (2) amphibole grown by a reaction with relict plagioclase and other lower-grade amphibole. In this case, as the plagioclase is richer in An than the expected metamorphic plagioclase, the equilibrium composition may be locally influenced by an anomalously high activity of Ca, producing an amphibole with a very low Na occupancy in M4.

Clinopyroxene

Clinopyroxene is an abundant phase in the normal amphibolites of the oceanic domain at the top of the pile (Fig. 5). However, in the quartz-rich amphibolites of the Hb zone, clinopyroxene is a very abundant mineral and occasionally the only ferromagnesian phase. For instance, the leucocratic bands of Fig. 4 are very rich in clinopyroxene and quartz whereas the adjacent normal amphibolites are free of clinopyroxene. This fact is in agreement with the experimental data reported by Spear (1981), from which the temperature of the clinopyroxene-in reaction is lowered if quartz is in excess in the system. Representative analyses of pyroxenes from these rock types are listed in Table 5.

The composition is very clustered around diopside that is poor in jadeite. For the pyroxenes coexisting with quartz in the leucocratic amphibolites, the quartz–jadeite equilibrium may be used to estimate pressures, as both phases are in textural equilibrium and crystallized together during the main episode of deformation. According to the calibration of Holland (1980), and for a temperature of ~750°C (the clinopyroxene-in temperature), a maximum pressure of ~2·5 kbar has been estimated.

WHOLE-ROCK CHEMISTRY

A selection of 28 samples has been made from the different facies that constitute the oceanic domain of the AMB: 22 samples correspond to normal amphibolites characterized by the common assemblage amphibole–plagioclase, and 6 samples correspond to the quartz-rich amphibolites appearing as centrimetre-sized bands alternating with the normal facies.

Table 4: Representative microprobe analyses of plagioclases

Rock type:	Cpx–Hb amphibolites			Hb amphibolites			Act–Hb amphibolites		
Sample:	893-22-10	893-24-14	893-25-4	893-28-5	893-30-8	893-31-4	893-39-9	893-40-4	893-41-3
SiO_2	58·70	56·59	53·68	55·03	59·31	59·41	54·91	57·73	57·01
Al_2O_3	25·41	27·03	28·66	27·00	25·06	25·20	27·09	25·98	25·85
FeO_t	0·37	0·17	0·23	0·12	0·17	0·27	0·38	0·11	0·13
MnO	0·00	0·00	0·02	0·00	0·00	0·00	0·00	0·01	0·01
MgO	0·00	0·08	0·00	0·06	0·10	0·06	0·00	0·03	0·00
CaO	8·09	9·86	11·95	10·34	7·46	7·54	10·53	9·13	9·19
Na_2O	7·00	5·79	4·40	5·53	7·14	6·94	5·23	6·64	6·87
K_2O	0·10	0·04	0·04	0·01	0·07	0·05	0·16	0·05	0·08
Total	99·66	99·65	99·14	98·15	99·38	99·47	98·32	99·86	99·12

Table 5: Representative microprobe analyses of pyroxenes

Rock type:	Normal amphibolites			Q-amphibolites		
Sample:	893-22-2	893-22-4	893-22-14	M72	M76	M78
SiO_2	52·61	51·93	52·38	52·75	52·67	52·39
TiO_2	0·05	0·21	0·22	0·07	0·08	0·10
Al_2O_3	0·90	1·51	1·38	0·90	1·02	0·96
Fe_2O_3*	0·93	1·41	0·00	0·00	0·00	0·00
FeO	7·45	7·60	9·10	9·38	9·73	9·31
MnO	0·25	0·27	0·30	0·39	0·43	0·42
MgO	12·69	12·51	12·27	12·73	12·76	12·95
CaO	24·56	23·30	23·82	23·05	23·26	23·18
Na_2O	0·29	0·49	0·00	0·49	0·49	0·58
K_2O	0·00	0·00	0·00	0·01	0·00	0·00
Total	99·62	99·23	99·46	99·76	100·43	99·88

*Recalculated.

For comparative purposes, representative samples from other metabasites appearing in the continental domain have been included in this study. These are (1) the Rellano amphibolites that alternate with marbles and calc-silicates (two samples), and (2) the mafic granulites (five samples) appearing in the high-temperature zone. These samples have been analysed for major and trace elements. Several representative samples have also been analysed for oxygen and neodymiun isotopes, with the aim of identifying the igneous nature or otherwise of these metabasitic rocks, as well as the nature of the source and any process related to their evolution.

Major and trace (Ba, Nb, Rb, Sr, Y and Zr) elements were determined by X-ray fluorescence (XRF) spectrometry at XRAL Laboratories of Canada. The lower reporting limit for major elements is 0·01% and for trace elements is 10 p.p.m. Precision for major element analyses is ±2% and for trace elements is less than ±5%. Inductively coupled plasma mass spectrometry (ICP-MS) at XRAL Laboratories was used for determination of REE, Th and U. The detection limits are 0·1 p.p.m. for La, Ce, Pr, Nd, Sm, Gd, Tb, Dy, Er, Tm, Yb, Th and U; and 0·05 p.p.m. for Eu, Ho and Lu.

Major and trace elements

A list of selected chemical analyses is given in Table 6. Figure 9 shows the silica variation diagrams. Normal amphibolites have major element signatures typical of tholeiitic basalts, whereas the quartz-rich amphibolites are richer in SiO_2, TiO_2, P_2O_5 and Na_2O but poorer in MgO and CaO. The Rellano amphibolites, intercalated within sediments of the continental domain, are very similar in composition (with the exception of silica) to the normal amphibolites of the oceanic domain. The samples from the mafic granulites—the pre-metamorphic intrusions of the continental domain—are very different in composition from the other mafic rocks of the AMB (Fig. 9). The salient feature of these mafic granulites is the high MgO content (up to 15 wt %) at high values of silica (>50 wt %). These values are typical of boninites, derived through the partial melting of an extremely depleted lithospheric mantle [see Crawford *et al.* (1981)]. All these metabasic rocks derive from the metamorphism of sub-alkaline magmatic rocks, as evidenced by the total alkalis to silica (TAS) ratio.

The contents of trace elements of petrogenetic interest, to be compared with typical MORBs using the normalization base of Pearce (1983), are listed in Table 6. The normal amphibolites have low contents of immobile incompatible elements typical of oceanic tholeiites (MORB). These values are extremely low in the mafic granulites for most of the selected elements. These relationships are well illustrated in the MORB-normalized spider diagrams (Fig. 10) (Pearce, 1983). Compared with MORB these mafic granulites have higher contents of Rb, Ba and K but lower concentrations of the high field strength elements (HFSE). The main geochemical features of these mafic granulites are the high MgO contents (up to 15·9%) and high silica contents (>50%). They are really high-Mg andesites with many similarities with the typical boninites as defined by Crawford *et al.* (1989).

Normal amphibolites from the oceanic domain have patterns similar to N-MORB for some immobile elements, but are enriched with respect to N-MORB in other elements such as Th and Nb.

Table 6: Whole-rock analyses of representative samples from metabasites of the Aracena metamorphic belt

Rock type:	Normal amphibolites								
Sample:	AL A 8 10	AL B 17 1	AL B 18 3	89322	89326	89327	89339	CO 2	CO 6
SiO_2	49·9	49·3	47·9	49·1	48·8	50·1	51·5	48·7	47·6
TiO_2	0·68	1·33	1·14	1·28	1·58	1·13	1·15	1·42	1·36
Al_2O_3	18·3	14·5	16·5	14·8	15·6	15·1	16·8	15·8	19·8
Fe_2O_{3t}	6·92	10·2	9·27	10·2	10·6	9·6	8·22	9·48	8·66
MgO	6·68	7·54	8·29	8·38	8·32	8·29	5·47	6·82	5·96
MnO	0·13	0·16	0·16	0·19	0·2	0·19	0·2	0·15	0·13
CaO	11·2	11·8	11·8	12·6	12·3	12·3	12·7	11	10·6
Na_2O	3·28	2·8	2·67	2·56	2·45	3·04	2·92	2·75	2·42
K_2O	0·1	0·07	0·11	0·06	0·01	0·01	0·54	0·42	0·41
P_2O_5	0·05	0·14	0·13	0·13	0·18	0·12	0·17	0·18	0·26
LOI	1	0·75	0·7	0·77	0·46	0·77	0·46	1·05	1·5
Total	98·24	98·59	98 67	100·07	100·5	100·65	100·13	97·77	98·7
Trace elements (p.p.m.)									
Cr	330	290	290	330	280	520	274	170	66
V	134	285	218	250	161	209	155	195	203
Sc	24·7	41·3	33·1	34	35	36	25	34·3	27·9
Ni	115	72	127	63	93	84	79	76	31
Co	36	42	44	29	35	33	27	37	34
Cu	70·3	11·5	48·9	36·3	36·6	9·4	47·3	58·2	53·3
Zn	50·2	35·3	56·2	34·6	47·3	32·3	57·3	63	50·8
Ba	26	n.d.	14	n.d.	n.d.	n.d.	169	91	n.d.
Rb	n.d.	20	n.d.	18	23	18	34	11	18
Sr	160	181	158	191	182	198	305	209	365
Y	30	18	19	22	31	24	25	30	n.d.
Th	4·9	n.d.	0·9	0·7	n.d.	n.d.	n.a.	1·4	n.d.
Zr	89	83	90	93	139	88	143	89	54
Hf	2·8	1·9	2·4	1·6	3·4	2·4	n.a.	2·7	1·4
Nb	n.d.	21	26	11	n.d.	13	n.d.	19	n.d.
La	5·9	5	5·3	5	4·6	3·8	13·6	7·4	6·3
Ce	14	13	14	14·3	15·5	12·8	31·4	18·3	15·2
Pr	n.a.	n.a.	n.a.	1·8	2·2	1·7	3·9	2·8	2·1
Nd	8	10	10	8·7	11·5	9·1	17	13·3	10
Sm	2·3	3	2·8	2·9	4	3·1	4·6	4·1	3·1
Eu	0·9	0·9	1·2	1·07	1·4	1·17	1·38	1·51	1·18
Gd	n.a.	n.a.	n.a.	3·2	4·4	3·5	4·9	4·2	3
Tb	0·5	0·6	0·5	0·6	0·8	0·6	0·8	0·8	0·5
Dy	n.a.	n.a.	n.a.	3·9	5·3	4·3	5·1	4·8	3·3
Ho	n.a.	n.a.	n.a.	0·82	1·09	0·88	1·03	1	0·63
Er	n.a.	n.a.	n.a.	2·4	3·1	2·6	3·1	2·8	1·8
Tm	n.a.	n.a.	n.a.	0·3	0·5	0·4	0·4	0·4	0·2
Yb	2·9	2·5	2·2	2·3	3	2·4	2·7	2·5	1·4
Lu	0·47	0·39	0·36	0·34	0·43	0·35	0·39	0·35	0·22

n.d., not determined; n.a., not analysed.

Table 6: continued

Rock type:	Q-amphibolites			Relíano		Granulites				
Sample:	AL A 8 9	AL B 17 3	AL B 19 1	CO 8	A29422A	89316	89318	89321	A2946	A2942
SiO_2	56·4	53·1	52·3	43·8	45·2	53·1	51	56·6	51·4	50·1
TiO_2	1·79	2·16	2·59	1·59	1·44	0·36	0·43	0·652	0·406	0·53
Al_2O_3	14·5	15·4	13·6	18·7	18·5	8·09	7·83	16·5	9·83	15·1
Fe_2O_{3t}	11·5	11	13·6	8·72	9·08	8·08	8·49	6·87	8·1	9·24
MgO	2·54	2·69	3·06	7·78	8·28	15	15·9	7·05	11·8	9·93
MnO	0·18	0·12	0·18	0·1	0·12	0·21	0·21	0·16	0·19	0·2
CaO	5·38	8·2	7·76	14·8	12·1	13·2	14·5	9·21	14·4	9·77
Na_2O	4·94	5·14	4·29	1·57	2·4	1 09	0·9	0·65	0·98	1·07
K_2O	0·07	0·06	0·06	0·42	1·01	0·75	0·59	0·66	0·66	1·62
P_2O_5	0·65	0·66	0·63	0·03	0·04	0·06	0·06	0·14	0·03	0·15
LOI	0·2	0·1	0·15	1·1	1·15	0·46	0·31	1·85	0·55	0·95
Total	98·15	98·63	98·22	98·61	97·88	100·04	99·79	99·69	97·94	98·13
Trace elements (p.p.m.)										
Cr	81	52	42	59	85	n.a	170	140	580	550
V	63	97	131	275	348	119	159	120	206	129
Sc	17·6	25·9	24·8	46·5	47	40	46	14	58	31
Ni	9	10	8	68	70	318	309	96	119	163
Co	25	26	28	49	36	54	57	25	33	31
Cu	296	6·6	15·3	77	37·4	129	125	68·1	13·8	13·2
Zn	56	27·4	30·3	43·2	51·8	66·2	49·9	30·1	47·6	69·9
Ba	n.d.	34	43	65	263	n.d.	n.d.	158	521	733
Rb	10	n.d.	n.d.	n.d.	20	42	35	30	21	49
Sr	174	210	194	347	297	157	160	260	146	258
Y	77	91	75	18	19	14	17	9	41	21
Th	4·5	6·4	4·1	n.d.	0·4	n.a.	n a.	7·3	1	1·5
Zr	505	437	397	46	76	23	n.d.	86	55	43
Hf	12	11	8·9	1·6	1·2	n.a.	0·4	6·6	1·5	1·1
Nb	27	13	51	20	9	17	12	19	3	6
La	25·2	18·7	22·6	3·8	4·9	5·2	4·8	11	6·3	8·8
Ce	60	46	59·6	10·1	12·8	15·3	16	26	18·9	19·6
Pr	n.a.	n.a.	8·6	1·6	1·9	2	2·2	2·7	3·2	2·7
Nd	34	33	42·7	8	9·4	9·2	10·4	9·9	17·4	12
Sm	9	8·9	13·6	2·9	3	3	3·1	2·3	6·4	3·5
Eu	3·1	3·1	3·86	1·12	0·97	0·7	0·65	0·66	1·1	0·86
Gd	n.a.	n.a.	14·7	2·8	3·2	3	3·2	2·4	6·9	3·5
Tb	1·7	2	2·6	0·5	0·6	0·5	0·5	0·3	1·3	0·6
Dy	n.a.	n.a.	16·7	3·2	3·5	3·1	3·3	2	7·9	3·9
Ho	n.a.	n.a.	3·54	0·67	0·73	0·58	0·65	0·35	1·61	0·79
Er	n.a.	n.a.	10·1	1·8	2·1	1·5	1·9	1	4·4	2·4
Tm	n.a.	n.a.	1·4	0·2	0·3	0·2	0·3	0·1	0·6	0·4
Yb	8·1	8·7	9·2	1·5	1·8	1·3	1·6	0·9	3·5	2·2
Lu	1·29	1·35	1·37	0·21	0·24	0·19	0·23	0·12	0·5	0·35

n.d., not determined; n.a., not analysed.

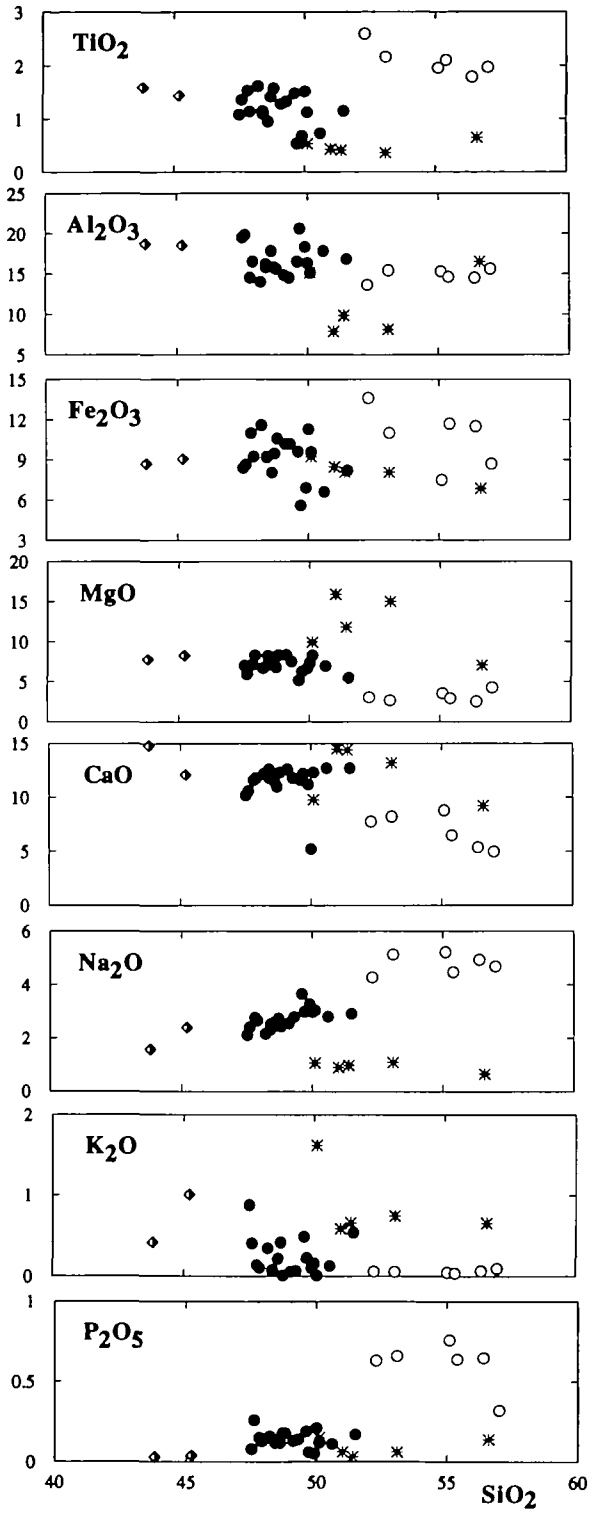

Fig. 9. Harker diagrams of the amphibolites from the oceanic domain. Solid circles: normal amphibolites. Open circles: quartz-rich amphibolites. For comparative purposes other metabasites from the continental domain have been represented. These are the El Rellano amphibolites (diamonds) and the mafic granulites (asterisks).

These features are intermediate between N-MORB and P-MORB (Saunders, 1984), suggesting that these amphibolites were derived from transitional-type MORBs.

On a chondrite-normalized plot (Fig. 11), most of the amphibolites from the oceanic domain display a nearly flat pattern with no Eu anomaly. Two samples display enrichment of LREE over HREE and no Eu anomaly. The quartz-rich amphibolites have a nearly flat pattern identical to that of the normal amphibolites but displaced to higher values. These patterns are characteristic of transitional tholeiites (T-MORB), which have intermediate features between normal and primitive MORBs (Saunders, 1984).

Neodymium isotopes

To determine the source nature of the studied metabasites (amphibolites and granulites) we have selected a set of representative samples from these rock types for Sm–Nd isotopes. Apart from the nature of the source region, the Nd isotope data will supply important information on the timing of magma generation in the ridge, from pairs of fractionation-related facies of amphibolites.

Five amphibolite samples have been analysed for Sm and Nd isotopes. Two samples are quartz-rich amphibolites collected from two separated layers alternating with normal amphibolites (Fig. 4) in the Hb-zone of the amphibolite unit. The other three samples correspond to normal amphibolites, two of which form pairs with the above-mentioned samples of quartz-rich amphibolites.

Nd isotope ratios were determined at SURRC, East Kilbride. Nd was separated from whole-rock powders using techniques described by Barbero *et al.* (1995), except that a modified procedure was adopted for the separation of Ba from the REE. The dried down bulk REE fraction collected from the cation exchange columns was dissolved in 3 M HNO_3 and loaded onto a column containing 2 ml of Eichrom Sr Spec resin (100–150 μm particle size). The REE were eluted with 3 M HNO_3, whereas Ba was retained on the column. Nd was separated from the other REE using the temperature-controlled anion exchange procedure of Barbero *et al.* (1995). No further purification was necessary. Samples were run on a VG Sector 54-30 thermal ionization mass spectrometer in multi-dynamic mode. $^{143}Nd/^{144}Nd$ ratios were corrected for mass fractionation using $^{146}Nd/^{144}Nd = 0{\cdot}7219$. During the course of this study the Johnson & Matthey Nd standard gave $^{143}Nd/^{144}Nd = 0{\cdot}511500 \pm 10$ (2 SD).

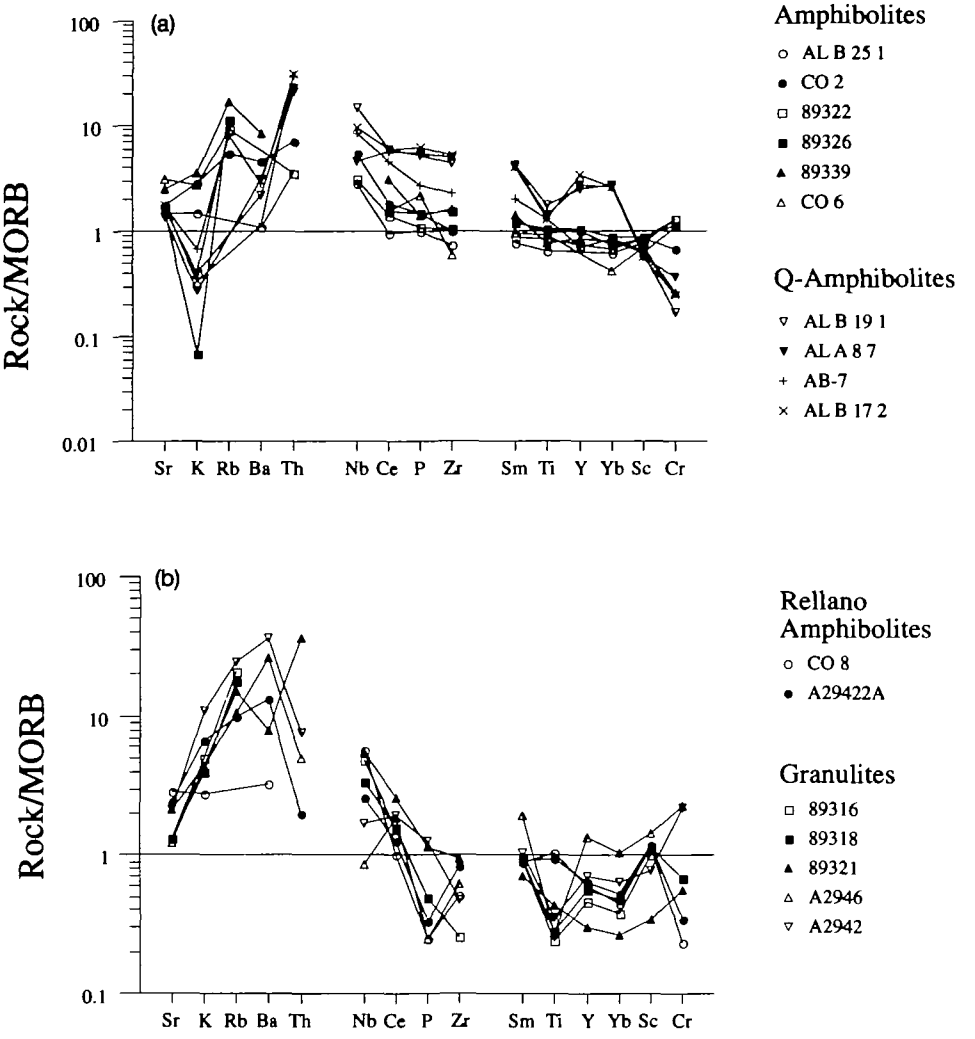

Fig. 10. Rock-MORB normalized spider-diagrams with representative samples of metabasites from the Aracena metamorphic belt.

Table 7 shows the Sm and Nd concentrations and the Nd isotope ratios of these samples. For every pair, the Nd isotope ratio of the quartz-rich amphibolite is lower than that of the respective normal amphibolite and the tie-lines linking every pair are parallel to one another (Fig. 12). This behaviour is in agreement with the fractionation process deduced from the whole-rock chemistry. The slope of these tie-lines may be related to the age of the fractionation process; however, this is poorly constrained because of the large errors resulting from the narrow range in the Sm/Nd ratios. Initial ε_{Nd} fall between +9·2 and +7·9, taking a minimum reference age of ~350 Ma according to the $^{40}Ar/^{39}Ar$ ages (Dallmeyer *et al.*, 1993) obtained for the metamorphism of the Aracena amphibolites. These values are typical of MORB (DePaolo, 1988).

Oxygen isotopes

The use of oxygen isotopes allows us to recognize the original position of the amphibolite slab in the oceanic crust. It is well documented from oxygen data of the Samail ophiolite in Oman (Gregory & Taylor, 1981) that only the uppermost part (2–3 km) of the oceanic crust is affected by seawater metasomatism. Oxygen isotope data from representative samples of the oceanic domain are listed in Table 8. These amphibolites display a wide range in the $\delta^{18}O$ (V-SMOW normalization) value from 3·7‰ to 8·8‰. This variation occurs in samples collected from the same outcrop and with minor differences in composition. It is typical of the hydrothermally altered oceanic crust, which may vary from 2·0‰ to 20‰ (Spooner *et al.*, 1974;

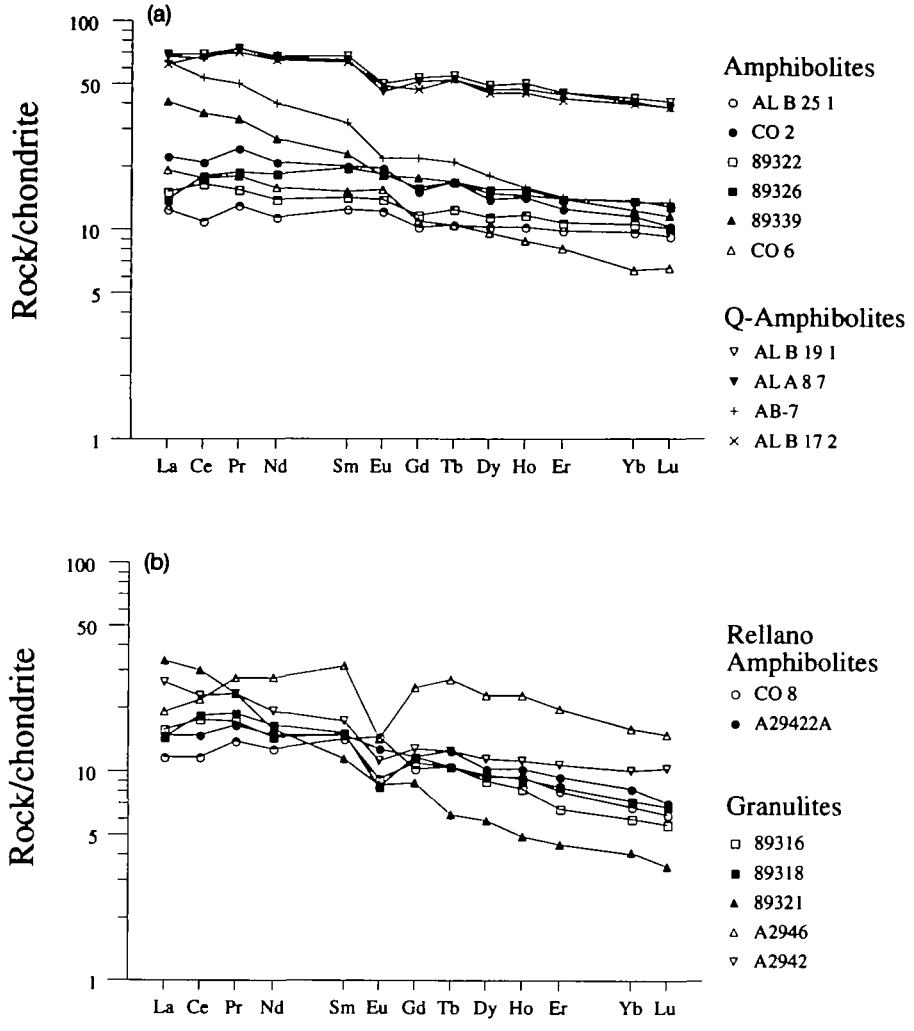

Fig. 11. Rock-chondrite normalized spider-diagrams with representative samples of metabasites from the Aracena metamorphic belt. Normalizing values from Nakamura (1974).

Table 7: Neodymium isotope analyses from selected samples of the amphibolite unit

Rock type	Sample	Sm (p.p.m.)	Nd (p.p.m.)	$^{147}Sm/^{144}Nd$	$^{143}Nd/^{144}Nd$	$\pm 2\sigma$	$(^{143}Nd/^{144}Nd)_{350}$	$\varepsilon_{Nd\ 350}$
Normal amph.	ALA8-10	2·3	8·0	0·1738	0·513022	11	0·512624	+8·5
Normal amph.	ALB17-1	3·0	10·0	0·1814	0·513073	17	0·512657	+9·2
Normal amph.	ALB18-3	2·8	10·0	0·1693	0·512981	12	0·512593	+7·9
Q-amph.	ALA8-9	9·0	34·0	0·1600	0·512965	7	0·512598	+8·0
Q-amph.	ALB17-3	8·9	33·0	0·1631	0·512995	6	0·512621	+8·5
	CHUR			0·1967	0·512638		0·512187	0·0

Table 8: Oxygen isotopes of amphibolites from the Aracena metamorphic belt

Sample	Assemblage	Rock type	$\delta^{18}O$
CO2	Hb–Pl–Il–Mt	Hb amphibolite	8·1
89322	Cpx–Hb–Pl–Il–Mt–Zr–Ap	Cpx–Hb amphibolite	4·7
89328	Hb–Pl–Il–Mt–Ap	Hb amphibolite	3·7
89332	Hb–Pl–Il–Mt	Hb amphibolite	3·9
89342	Hb–Pl–Il–Mt–Ep	Hb amphibolite	7·6
89339	Hb–Pl–Il–Mt–Ep	Hb amphibolite	8·8
AL 9228	Hb–Pl–Il–Mt	Hb amphibolite	8·8
CO6	Hb–Pl–Il–Mt	Hb amphibolite	7·3
AL B 17 2	Hb–Pl–Q–Il–Mt–Sph–Ap–Zr	Q–amphibolite	5·5

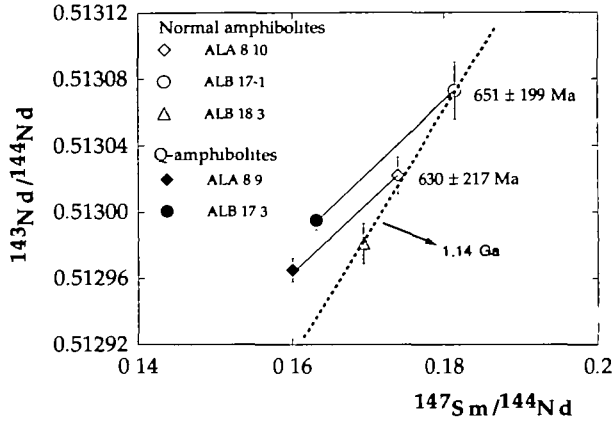

Fig. 12. $^{143}Nd/^{144}Nd$ vs $^{147}Sm/^{144}Nd$ diagram plotting selected samples of amphibolites and quartz-rich amphibolites (see text).

Gregory & Taylor, 1981), although this wide range is reduced in the course of subduction (Hoefs, 1987), as the fluids expelled during prograde reactions tend to homogenize the resulting amphibolite pile.

DISCUSSION

Petrogenesis of metabasites

Both REE and ε_{Nd} data strongly support an origin from mid-ocean ridge magmatism for the amphibolites from the Aracena metamorphic belt. If we consider jointly the three normal amphibolites analysed for Nd isotopes, they display a good straight correlation (Fig. 12). The meaning of this correlation is not very well constrained by this study. However, it may be the result of an isotope homogenization that occurred in the mantle source 1·14 Ga ago, the age obtained taking this correlation as an isochron. This implies that the isotope homogenization occurred around 600 Ma before the partial melting event that produced the oceanic crust. This time interval is in agreement with the estimations by DePaolo (1988) based on the small total range of the ε_{Nd} data, within 12 units, and the expected percentages of partial melting from the peridotite source.

The relationships between normal amphibolites and quartz-rich amphibolites are complex, so, on one hand, the relative enrichment in the major oxides is compatible with a fractionation process from a tholeiite composition, although, on the other hand, the samples are not aligned on a single, continuous trend similar to a liquid-line of descent. By contrast, both groups show separated but parallel trends for most of the major oxides (Fig. 9). As quartz-rich amphibolites and normal amphibolites are associated in layers within the amphibolite pile of the oceanic domain, we have sampled several pairs from selected outcrops. It is interesting to note that the lines linking pairs of amphibolites from separated outcrops are parallel, as depicted in Fig. 13a and b for the cases of TiO_2 and P_2O_5, respectively. This behaviour is identical for several trace elements, as depicted in Fig. 13c and d for the cases of a typical refractory element (Cr) and an incompatible immobile element (Zr), respectively. This behaviour supports the existence of a multiple fractionation process from a set of parental magmas. It implies the existence of a multi-chamber system beneath the ridge; every magma chamber having a composition similar to the adjacent chambers, and all the chambers undergoing similar fractionation processes to separated closed systems.

This fractionation process accounts for the REE enrichment of the quartz-rich amphibolites. An alternative mechanism for REE enrichment in these amphibolites, based on differential rates of partial melting, is inconsistent with the transitional character (T-MORB) of these melts. A low rate of

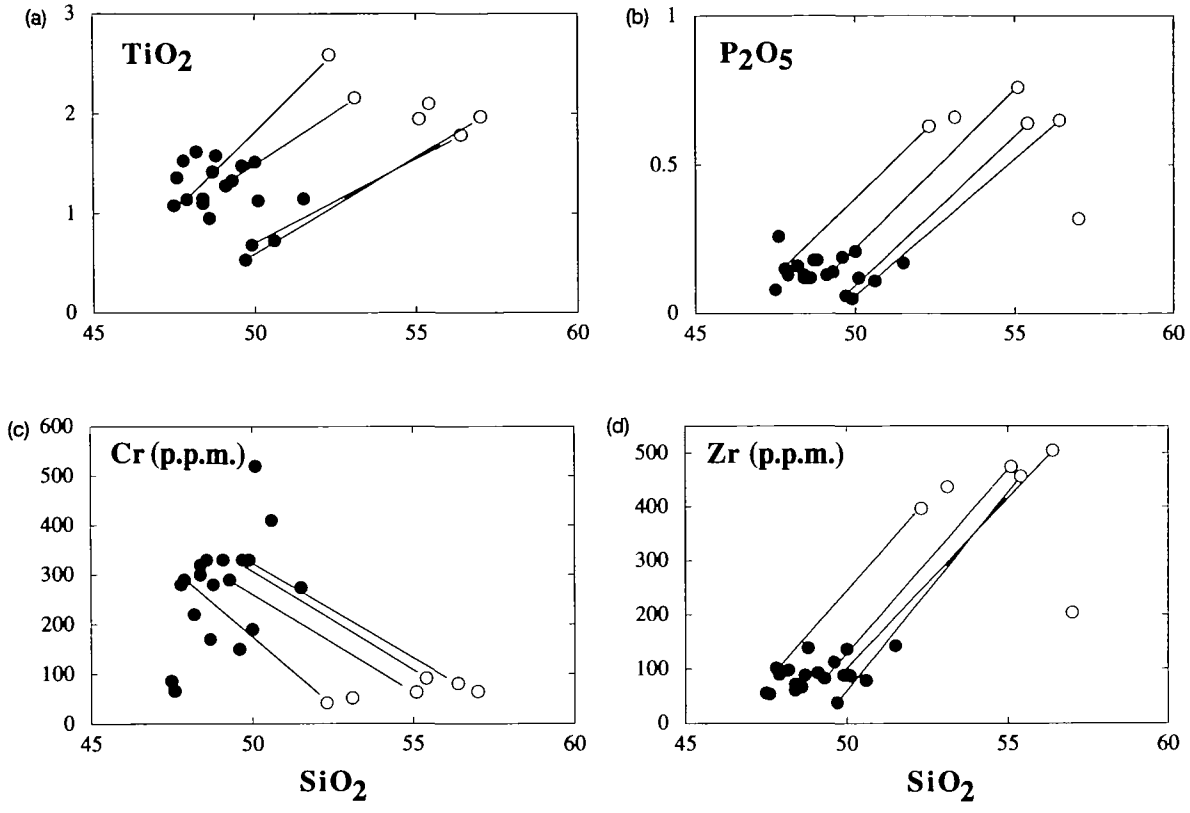

Fig. 13. Silica variation plots for major and trace elements, showing the relationships between normal and quartz-rich amphibolites. Tie-lines link pairs of samples from two adjacent bands.

partial melting for the peridotite source would produce REE-rich melts but with a non-flat pattern; this will be positive or negative depending on the normal or primitive character of the source. Figure 14 shows the Aracena metabasites plotted on a Ce_n/Yb_n vs Yb_n (n denotes chondrite-normalized values) diagram with the main fields of normal, transitional and primitive MORBs. Most of the normal amphibolites from the oceanic domain plot in the field of T-MORB and only a few plot near the field of P-MORB. The quartz-rich amphibolites plot outside from the MORB fields and away from the partial melting trend calculated for a garnet lherzolite source (Saunders, 1984).

The variations observed in the $\delta^{18}O$ values may be due to distinct processes. On one hand, the increase in $\delta^{18}O$ is parallel to the increase in mobile incompatible elements. It may be the result of hydrothermal alteration during seawater interaction. This alteration may affect the upper 2–3 km of the oceanic crust (McCulloch & Taylor, 1980; Gregory & Taylor, 1981), giving rise to very heterogeneous distributions of the altered zones, as these are related to fluid circulation through fractures in the basalt pile (Peacock, 1993). These altered zones are enriched in mobile incompatible elements dissolved in the seawater. The newly formed minerals resulting from the alteration process record a high $\delta^{18}O$ value in equilibrium with the seawater. Other relict

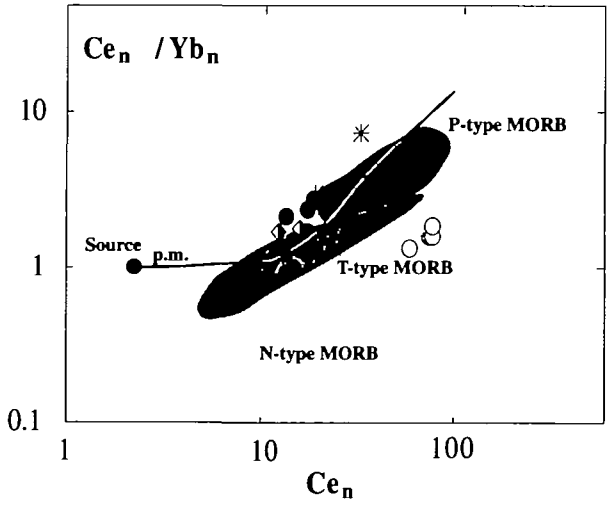

Fig. 14. Ce/Yb vs Yb (normalized values) showing the disposition of the Aracena metabasites compared with the MORB types (symbols as in Fig. 9). The fields for N-, P- and T-type MORB are drafted from single data point compiled by Saunders (1984).

minerals, not affected by this process, retain the original low $\delta^{18}O$ values, giving rise to the observed heterogeneity, which depends on the intensity of the alteration process. On the other hand, alteration by fluids related to the retrograde metamorphism and the interaction with continental sediments, during the late exhumation of the amphibolite pile, also may cause the $\delta^{18}O$ value to increase but with no parallel enrichment with respect to mobile large ion lithophile elements (LILE). These data are in agreement with an oceanic provenance of the amphibolites, and indicate that they come from the metamorphism and late exhumation of the uppermost part of an oceanic crust. This is crucial for the proposed tectonic model, as other possible models, such as obduction of an oceanic slab, are ruled out.

The amphibolites interlayered with marbles and calc-silicates in the continental domain (the Rellano amphibolites) are very similar in composition to the normal amphibolites of the oceanic domain. They are remnants of an initial stage of rifting before the development of the ocean represented by the amphibolites of the oceanic domain. The mantle source for both types of basalts was probably the same, as indicated by the geochemical signatures mentioned above.

The mafic granulites, intruded as pre-metamorphic bodies into the pelitic migmatites of the continental domain, represent andesite magmas of boninite affinity. Though many of these rocks have a metamorphic texture, some facies retain their original igneous textures. These igneous facies are very rich in low-Ca pyroxenes. The metamorphism of these igneous rocks is essentially a textural change, as the mineralogy and whole-rock chemistry are not modified. The facies with typical igneous textures have no signs of being igneous cumulates, so we conclude that the geochemical signatures come from the andesite magma from which they crystallized. However, the contents in LILE, though being lower than for typical MORB (Fig. 10), are slightly higher than for typical boninites. This feature is more marked for mobile LILE, but also is appreciable for some HFSE (Fig. 10). These aspects may result from the influence of fluids released by the subducting slab that metasomatized the harzburgite source region for boninite magmatism [see Hickey & Frey (1982) and Crawford *et al.* (1989)].

The fluids released from the down-going slab metasomatize the adjacent lithospheric mantle wedge, transforming this region of the sterile mantle lithosphere into a potentially fertile harzburgite. Cessation of subduction may be a way to promote a thermal rebound, in this metasomatized wedge, reaching the wet peridotite solidus and producing the boninite magmatism. Another mechanism to induce the thermal rebound is the subduction of a ridge with the consequent creation of a slab-free window (Rogers & Saunders, 1989; Hole *et al.*, 1991). In the Crawford *et al.* (1981) model, the reactivation of the lithospheric mantle is induced by the ascent of a peridotite diapir beneath the subduction-related volcanic arc. The proximity of boninite rocks to the oceanic domain in the AMB, as well as the continental nature of the host into which these magmas intruded, are arguments against any relation with a volcanic-arc setting. Cessation of subduction is unlikely because of the preservation of an inverted metamorphic gradient in the oceanic domain of the AMB, for which it is necessary that subduction continues after the main episode of metamorphism.

Thermal evolution of the oceanic domain

The absence of garnet in the amphibolites from the oceanic domain, together with the absence of epidote in the hornblende–plagioclase facies, indicates that these rocks equilibrated at low pressures. The pressure estimated from the jadeite content in clinopyroxene is $<2{\cdot}5$ kbar as calculated for the quartz-rich amphibolites, in which the quartz–jadeite–albite equilibrium may be applied. This pressure is coincident with that obtained by comparison with the experimental data of Spear (1981). The equilibrium temperature varies across the amphibolite pile, increasing from south to north, from the greenschist–amphibolite facies transition ($\sim$550°C) up to the amphibolite–granulite facies transition (Fig. 2). The temperature of this amphibolite–granulite facies transition is estimated at $\sim$780°C according to the experimental data of Spear (1981). This variation in temperature occurs across a narrow band of no more than 500 m, implying a metamorphic gradient of $\sim$460°C/km. Because the metamorphic foliation, the contacts of the amphibolite pile and the isograds dip towards the north, this gradient is inverted; that is, with the temperature increasing upwards. An alternative explanation, implying tectonic inversion, by folding and/or stacking of the amphibolite pile may be ruled out, based on structural data. These include the differences in tectonic style between the oceanic and continental domains: the axial traces of folds within the continental domain are crosscut by the contact with the oceanic domain, in which the main phase of deformation is by shearing. Both episodes of deformation occurred at the same time and may be kinematically compatible with the same tectonic process, but the amphibolite slab is not geometrically

linked with inverted limbs of folds in the continental domain. The second metamorphic episode is associated with discrete shear bands developed within the amphibolite pile, but especially concentrated at the southern and northern margins of the pile. During this episode of deformation (OD-D_2), retrogression of the pre-existing assemblages to greenschist facies occurred.

Tectonic model

The inverted metamorphic gradient of the oceanic domain is the typical thermal structure found in subduction-related complexes such as the Pelona–Orocopia complex of the Western Cordillera in California (Graham & England, 1976; Peacock, 1987). The inverted metamorphic gradient can be a consequence of dynamic advection related to subduction, and shear heating along the subduction thrust. Both factors contribute to heat transfer from the hanging wall to the oceanic slab.

However, the inverted metamorphic gradient of the AMB is greater than those reported in subduction-related complexes [see Peacock (1987)]. Another difference between these complexes and the AMB is the high pressure (>8 kbar) compared with the low-pressure regime of the AMB. The thermal structure of the continental hanging wall, at the time of subduction, may be responsible for the low-pressure, inverted-gradient metamorphism experienced by the slab. This implies that the continental hanging wall must be heated immediately before slab subduction. Evidence for this anomalous heating of the continental block is documented by the low-pressure–ultra-high-temperature regime observed over a narrow and linear band in the continental domain of the AMB. Furthermore, the presence of pre-metamorphic intrusions of Mg-rich andesite magmas with boninite affinities in the CD is evidence for the partial melting of the lithospheric mantle beneath the continental margin at the time of subduction.

Geochemical and petrogenetic features, as well as the thermal evolution of the AMB suggest the following scenario (Fig. 15):

(1) Subduction of an oceanic lithosphere beneath the CD. Dehydration of the down-going slab induced the metasomatism of the overlying lithospheric mantle (Fig. 15a).

(2) The ridge subduction deduced from this study, with the development of a slab-free window, implies the migration of the triple junction along the edge of the CD. It promoted the upwelling of the underlying asthenosphere, and a thermal rebound developing a high-T belt in the upper plate above the slab window. This increase in temperature induced partial melting of the metasomatized lithospheric mantle wedge under the continental margin, with the genesis of boninite magmatism (Fig. 15b).

(3) Hot subduction of the western plate under the thermal anomaly created an inverted metamorphic gradient in the top of the oceanic slab (Fig. 15c).

(4) In a later stage, the upper slice of the sub-

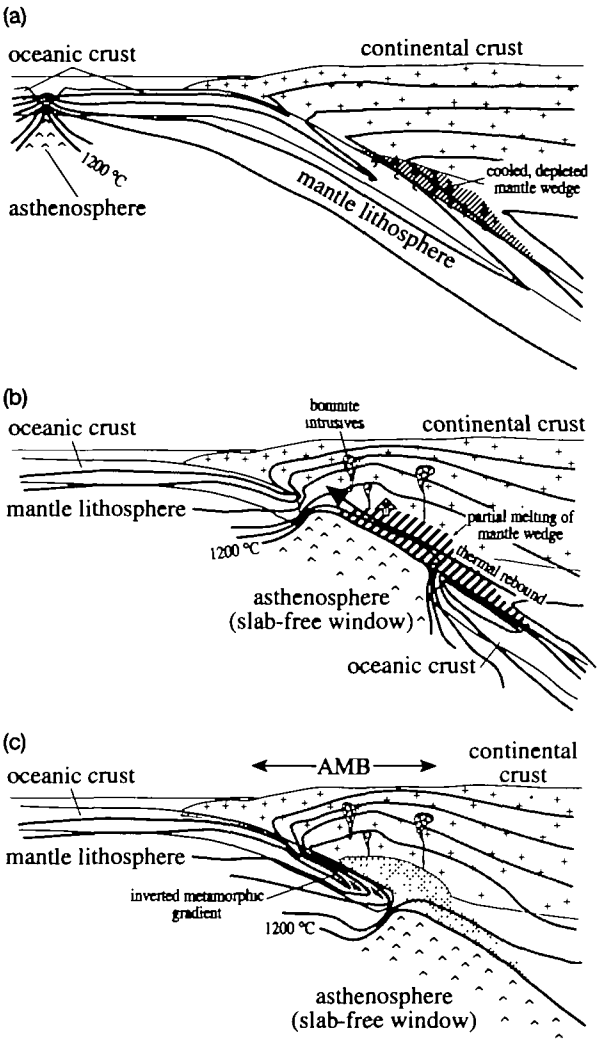

Fig. 15. Schematic tectonic model for the Aracena metamorphic belt. The migration of a triple junction along the edge of the Gondwana plate (a) produces the consumption of an intermediate oceanic plate, the opening of a slab window, and the upwelling of the underlying asthenosphere. As a result, a high-T belt develops in the continental margin, the AMB (b). Bodies with dot patterns represent boninitic intrusions. Subduction of the western plate under the thermal anomaly creates an inverted metamorphic gradient in the top of the oceanic slab. In a later stage (c), the upper slice of the subducting slab is incorporated into the continental margin. The process involves the downwards migration of the plate boundary, and the partial subduction of the accretionary prism, overthrust by the amphibolite slice. As a consequence, a greenschist-facies retromorphism develops in the amphibolite pile.

ducting slab was accreted to the base of the continental margin. The process involved the downward migration of the plate boundary and the partial underthrusting of the accretionary prism, producing the uplift rate required to preserve the inverted metamorphic gradient [see Peacock (1987)].

CONCLUSIONS

The Aracena metamorphic belt represents a low-pressure–high-temperature subduction complex in which metamorphism of the subducting oceanic slab was induced from the previously heated continental hanging wall. This anomalous heating occurred as a consequence of thermal rebound associated with subduction of the ridge and the creation of a slab-free window. This tectonic model is supported by three petrological features: (1) the low-pressure inverted metamorphic gradient of amphibolites of the oceanic domain; (2) the high-temperature–low-pressure metamorphism of the continental hanging wall; (3) the early intrusion of boninites into the continental domain. These features confer a special relevance to the Aracena metamorphic belt. They may be used as indirect criteria for recognizing ancient subduction zones in which the typical signatures such as blueschist metamorphism are absent. The Aracena metamorphic belt may be taken as a model example for atypical subduction settings in ancient orogenies.

ACKNOWLEDGEMENTS

This paper considerably benefited from the constructive criticisms by Dr T. Rushmer and Dr R. Rudnick. This study is part of the AROCHE (Análisis de la Rama Oeste de la Cadena Hercínica Europea) project funded by the Spanish Ministry of Education and Science (CICYT-DGICYT, Project PB91-0600), by the Andalusian Government (Projects PAI-4018 and PAI-4108) and the University of Huelva.

REFERENCES

Abalos, B., Gil Ibarguchi, I. & Eguiluz, L., 1991. Structural and metamorphic evolution of the Almaden de la Plata Core (Sevilla, Spain) in relation to syn-metamorphic shear between the Ossa–Morena and South Portuguese zones of the Iberian Variscan fold belt. *Tectonophysics* **191**, 365–387.

Barbero, L., Villaseca, C., Rogers, G. & Brown, P. E., 1995. Geochemical and isotopic disequilibrium in crustal melting: an insight from the anatectic granitoids from Toledo (Spain). *Journal of Geophysical Research* **100**, 15745–15765.

Bard, J. P., 1969. Le métamorphisme régional progressif de Sierra de Aracena en Andalousie occidentale (Espagne). Thèse d'Etat, University of Montpellier, 398 pp.

Bard, J. P., 1992. Les complexes intrusifs acide–basique calco-alcalines de la Chaîne Varisque Sud-Iberique et leurs liaisons avec les grands cisaillements transpressifs de Badajoz–Cordoue et de la Zone Sud-Iberique: proposition de modèles géodynamiques impliquant des processus de subduction continentale. *Comptes Rendus Hebdomadaires des Séances de l'Académie des Sciences* **314**, 711–716.

Bard, J. P. & Moine, B., 1979. Acebuches amphibolites in the Aracena Hercynian metamorphic belt (southwest Spain): geochemical variations and basaltic affinities. *Lithos* **12**, 271–282.

Blundy, J. D. & Holland, J. B., 1990. Calcic amphibole equilibria and a new amphibole–plagioclase geothermometer. *Contributions to Mineralogy and Petrology* **104**, 208–224.

Blundy, J. D., Brodholt, J. P. & Wood, B. J, 1991. Carbon–fluid equilibria and the oxidation state of the upper mantle. *Nature* **349**, 321–324.

Carmichael, I. S. E. & Nicholls, J., 1967. Iron–titanium oxide and oxygen fugacities in volcanic rocks. *Journal of Geophysical Research* **72**, 4665–4687.

Crawford, A. J., Beccaluva, L. & Serri, G., 1981. Tectonomagmatic evolution of the West Philippine–Mariana region and the origin of boninites. *Earth and Planetary Science Letters* **54**, 346–356.

Crawford, A. J., Falloon, T. J. & Green, D. H., 1989. Classification, petrogenesis and tectonic setting of boninites. In: Crawford, A. J. (ed.) *Boninites and Related Rocks*. London: Unwin Hyman.

Crespo-Blanc, A., 1987. El macizo de Aracena (macizo Ibérico meridional): propuesta de división sobre la base de nuevos datos estructurales y petrográficos. *Boletín Geológico y Minero* **98**, 507–515.

Crespo-Blanc, A. & Orozco, M., 1988. The Southern Iberian Shear Zone: a major boundary in the Hercynian folded belt. *Tectonophysics* **148**, 221–227.

Dallmeyer, R. D., Fonseca, P. E., Quesada, C. & Ribeiro, A., 1993. $^{40}Ar/^{39}Ar$ mineral age constraints for the tectonothermal evolution of a Variscan suture in southwest Iberia. *Tectonophysics* **222**, 177–194.

DePaolo, D. J., 1988. *Neodymium Isotope Geochemistry. An Introduction*. Berlin: Springer-Verlag, 187 pp.

Dupuy, C., Dostal, J. & Bard, J. P., 1979. Trace element geochemistry of Paleozoic amphibolites from SW Spain. *Tschermaks Mineralogische und Petrographische Mitteilungen* **26**, 87–93.

Eden, C., 1991. Tectonostratigraphic analysis of the northern extent of the oceanic exotic terrane, northwestern Huelva province, Spain. Ph.D. Thesis, University of Southampton.

Graham, C. M. & England, P. C., 1976. Thermal regimes and regional metamorphism in the vicinity of overthrust faults: an example of shear heating and inverted metamorphic zonation from southern California. *Earth and Planetary Science Letters* **31**, 142–152.

Gregory, R. T. & Taylor, H. P., 1981. An oxygen isotope profile in a section of Cretaceous oceanic crust, Samail ophiolite, Oman: evidence for $\delta^{18}O$ buffering of the oceans by deep (5 km) sea water–hydrothermal circulation at mid-ocean ridges. *Journal of Geophysical Research* **86**, 2737–2755.

Hickey, R. L. & Frey, F. A., 1982. Geochemical characteristics of boninite series volcanics: implications for the source. *Geochimica et Cosmochimica Acta* **46**, 2099–2115.

Hoefs, J., 1987. *Stable Isotope Geochemistry*. Berlin: Springer-Verlag, 241 pp.

Hole, M. J., Rogers, G., Saunders, A. D. & Storey, M., 1991. Relation between alkalic volcanism and slab-window formation. *Geology* **19**, 657–660.

Holland, T. J. B., 1980. The reaction albite = jadeite + quartz determined experimentally in the range 600–1200°C. *American Mineralogist* **65**, 129–134.

Hyndman, D. W., 1972. *Petrology of Igneous and Metamorphic Rocks*. New York: McGraw–Hill, 533 pp.

Julivert, M., Fontboté, J. M., Ribeiro, A. & Conde, L. N., 1974. Memoria explicativa del Mapa Tectónico de la Península Ibérica y Baleares. Madrid: IGME.

Laird, J., 1980. Phase equilibria in mafic schists from Vermont. *Journal of Petrology* **21**, 1–37.

Laird, J. & Albee, A. L., 1981. Pressure, temperature and time indicators in mafic schist: their application to reconstructing the polymetamorphic history of Vermont. *American Journal of Science* **281**, 127–175.

Leake, B. E., 1978. Nomenclature of amphiboles. *Canadian Mineralogist* **16**, 501–520.

McCulloch, M. T., & Taylor, H. P., 1980. A neodymium, strontium, and oxygen isotopic study of the Cretaceous Samail ophiolite and implications for the petrogenesis and seawater–hydrothermal alteration of oceanic crust. *Earth and Planetary Science Letters* **46**, 201–211.

Miyashiro, A., 1973. *Metamorphism and Metamorphic Belts*. London: George Allen & Unwin, 492 pp.

Moody, J. B. M. D. & Jenkins, J. E., 1983. Experimental characterization of the greenschist/amphibolite boundary in mafic systems. *American Journal of Science* **283**, 48–92.

Nakamura, N., 1974. Determination of REE, Ba, Mg, Na and K in carbonaceous and ordinary chondrites. *Geochimica et Cosmochimica Acta* **38**, 757–773.

Peacock, S. M., 1987. Creation and preservation of subduction-related inverted metamorphic gradients. *Journal of Geophysical Research* **92**, 12763–12781.

Peacock, S. M., 1993. The importance of blueschist–eclogite dehydration reactions in subducting oceanic crust. *Geological Society of America Bulletin* **105**, 684–694.

Pearce, J. A., 1983. The role of the sub-continental lithosphere in magma genesis at destructive plate margins. In: Hawkesworth, C. J. & Norry, M. J. (eds) *Continental Basalts and Mantle Xenoliths*. Nantwich, UK: Shiva, pp. 230–249.

Pe-Piper, G., 1988. Calcic amphiboles of mafic rocks of the Jeffers Brook plutonic complex, Nova Scotia, Canada. *American Mineralogist* **73**, 993–1006.

Quesada, C., 1991. Geological constraints on the Paleozoic tectonic evolution of tectonostratigraphic terranes in the Iberian Massif. *Tectonophysics* **185**, 225–245.

Quesada, C., Fonseca, P. E., Munhá, J., Oliveira, J. T. & Ribeiro, A., 1994. The Beja–Acebuches Ophiolite (Southern Iberia Variscan fold belt): geological characterization and geodynamic significance. *Boletin Geologico y Minero* **105**, 3–49.

Robinson, P., Spear, F. S., Schumacher, J. C., Laird, J., Klein, C., Evans, B. W. & Doolan, B. L., 1982. Phase relations of metamorphic amphiboles: natural occurrences and theory. *Mineralogical Society of America, Reviews in Mineralogy* **277**, 1–277.

Rogers, G. & Saunders, A. D., 1989. Magnesian andesites from Mexico, Chile and the Aleutian Islands: implications for magmatism associated with ridge–trench collisions. In: Crawford, A. J. (ed.) *Boninites and Related Rocks*. London: Unwin Hyman, pp. 416–445.

Saunders, A. D., 1984. The rare earth element characteristics of igneous rocks from the ocean basins. In: Henderson, P. (ed.) *Rare Earth Element Geochemistry*. Amsterdam: Elsevier, pp. 205–236.

Spear, F. S., 1980. NaSi–CaAl exchange equilibrium between plagioclase and amphibole. An empirical model. *Contributions to Mineralogy and Petrology* **72**, 33–41.

Spear, F. S., 1981. An experimental study of hornblende stability and compositional variability in amphibolite. *American Journal of Science* **281**, 697–734.

Spear, F. S., 1982. Phase equilibria of amphibolites from the Post Pond Volcanics, Mt Cube Quadrangle, Vermont. *Journal of Petrology* **23**, 383–426.

Spooner, E. T. C., Beckinsale, R. D., Fyfe, W. S. & Smewing, J. D., 1974. ^{18}O-enriched ophiolite metabasic rocks from E Liguria (Italy), Pindos (Greece) and Troodos (Cyprus). *Contributions to Mineralogy and Petrology* **47**, 41–62.

Trzienski, W. E., Carmichael, D. M. & Helmstaedt, H., 1984. Zoned sodic amphibole: petrologic indicator of changing pressure and temperature during tectonism in the Bathurst Area, New Brunswick, Canada. *Contributions to Mineralogy and Petrology* **85**, 311–320.

RECEIVED JANUARY 23, 1995
REVISED TYPESCRIPT ACCEPTED SEPTEMBER 11, 1995

APPENDIX: THE AMPHIBOLE COMPOSITION SPACE

The main problem in investigating the amphibole composition space is to find a set of linearly independent phase components with which all the possible chemical changes in the amphibole molecule may be modelled. For calcic amphiboles, such as those found in the Aracena amphibolites, the composition space can be *a priori* modelled with the additive component tremolite (Tr) and several molecules that result from the application of the exchange components, as shown in Table A1.

Table A1

Phase component	Exchange vector	End-member molecule
Tremolite	—	$Ca_2Mg_5Si_8O_{22}(OH)_2$
Edenite	$AlNaSi_{-1}\square_{-1}$	$NaCa_2Mg_5Si_7AlO_{22}(OH)_2$
Tschermakite	$Al_2Si_{-1}Mg_{-1}$	$Ca_2Mg_3Al_2Si_6Al_2O_{22}(OH)_2$
Glaucophane	$AlNaMg_{-1}Ca_{-1}$	$Na_2Mg_3Al_2Si_8O_{22}(OH)_2$
Ti-Tschermakite	$Al_2TiSi_{-2}Mg_{-1}$	$Ca_2Mg_4TiAl_2Si_6O_{22}(OH)_2$

The composition space is defined by the oxides SiO_2–Al_2O_3–FeO–MgO–TiO_2–CaO–Na_2O. The space can be condensed through $FeMg_{-1}$, resulting in a six-dimension condensed space (SAFTCN) in which the above-mentioned exchange components and the additive component Tr can be modelled. In theory, any calcic amphibole can be expressed in terms of these end-members and the Tr additive component by algebraic transformation of the composition space. However, a sixth molecule or exchange component must be added to proceed with the algebraic transformation. A plagioclase component must be used, and it is justified as most of the changes in the amphibole composition are paralleled by changes in the plagioclase composition through the plagioclase exchange that operates between Gl–Ts and Ab–An [see Spear (1980, 1981)].

However, if the plagioclase exchange vector $NaSiCa_{-1}Al_{-1}$ is considered as a component of the amphibole space composition, the component matrix cannot be transformed, as there is a linear dependence between Gl and Pl, or between Ts and Pl. No other exchange component can be added, as the space is constrained for calcic and calcosodic amphiboles, occupancy in the M4 site being dominated by Ca (at >90%). The proportion of the $MgCa_{-1}$ exchange, reduced as a consequence of the cummingtonite–hornblende solvus, does not occur in the amphiboles of the Aracena amphibolites. The plagioclase exchange relating Gl and Ts in amphiboles is coupled by the same exchange as that relating Ab and An in plagioclases. In other words, the plagioclase exchange in the amphibole molecule in relation to changing P and T is only possible if a parallel change in the anorthite content of the plagioclase occurs. This implies the existence of a net-transfer reaction defined by the plagioclase exchange

$$2(NaAlSi_3O_8) + Ca_2Mg_5Al_4Si_6O_{22}(OH)_2 = Na_2Mg_5Al_2Si_8O_{22}(OH)_2 + 2(CaAl_2Si_2O_8).$$

albite + tschermakite = glaucophane + anorthite

The existence of this net-transfer reaction is of great relevance, as it implies changes in volume and entropy and can be used in thermometry and barometry (Spear, 1980). For our purposes, it means that plagioclase must be considered as an 'external component' of the amphibole molecule. The proportion of plagioclase in the amphibole molecule must be zero if the assumed anorthite content satisfies chemical and thermodynamic equilibrium within the amphibole molecule. In our case, we take as a reference a plagioclase of 50 mol% in anorthite constant composition (the most usual composition of the analysed samples) and introduce it into the composition space together with the additive component Tr and the end-members Gl, Ts, Ti-Ts and Ed. The input matrix and the transformation matrix are listed in Table A2. If an amphibole has a negative value for the plagioclase content it means that the assumed composition of An_{50} is not the real composition at equilibrium. This fixed composition may appear as underestimated (negative) for high-temperature amphiboles or overestimated (positive) for low-temperature amphiboles. Furthermore, as the Ts, Ti-Ts and Ed exchanges are strongly dependent on temperature (Spear, 1981; Blundy & Holland, 1990) and Gl on pressure, the variations in both molecules may be used as a guide to determine the shape of the P–T path.

Table A2: Input and inverted matrix for the amphibole space composition

Input matrix

8·0	8·0	6·0	6·0	7·0	2·5	Gl	=	S
2·0	0·0	4·0	2·0	1·0	1·5	Tr		A
3·0	5·0	3·0	4·0	5·0	0·0	Ts		F
0·0	0·0	0·0	1·0	0·0	0·0	Ti-Ts		T
0·0	2·0	2·0	2·0	2·0	0·5	Ed		C
2·0	0·0	0·0	0·0	1·0	0·5	$Pl(An_{50})$		N

Inverted matrix

0·063	0·094	0·125	0·063	−0·563	−0·031	S	=	Gl
0·250	−0·208	−0·167	−0·250	−0·083	−0·542	A		Tr
−0·063	0·323	0·208	−0·563	−0·271	−0·385	F		Ts
0·000	0·000	0·000	1·000	0·000	0·000	T		Ti-Ts
−0·250	−0·042	0·167	−0·250	0·583	0·792	C		Ed
0·250	−0·292	−0·833	0·250	1·083	0·542	N		$Pl(An_{50})$